Chapter 1: Overview of Nanometer-sized Materials

1.1 General introduction

Properties of bulk materials with micrometer sizes or larger have been investigated widely and are well understood. Recently, nanometer-sized materials, such as colloidal semiconductor quantum dots (QDs, 1~10 nm), noble-metal nanoparticles (NPs, 10~100 nm) and noble-metal nanoclusters (NCs, < 1nm), have attracted much attention due to unique optical properties for a variety of applications in physics, chemistry, and biology, including biological labeling, sensing, and optoelectronic devices.[1~5] They bridge the gap between molecules and bulk materials. These nanomaterials, with sizes ranging from subnanometer to ~100 nm, exhibit distinct properties from corresponding bulk materials. On this scales, the optical and electronic behavior strongly depends on sizes, called quantum size effects due to localization of the carriers. For example, the emission color from colloidal CdSe QDs can cover the whole visible range by only changing the QD sizes. Moreover, many of the atoms are still located on the surface, thus surface effect is gradually important as decreases of the particle sizes due to increases of surface to volume ratios. The nanometer scale is also important and interesting in biological systems. Many biological systems, such as protein and DNA, have sizes comparable to these nanometer-sized materials. Therefore, we can probe and obtain some interesting and useful information by incorporating nanometer-sized materials into biological systems.

For investigating nanometer-sized materials, the optical and electronic microscopy has been used widely. An important advance in optical microscopy is the direct observation of single nano-objects within the ensemble nanomaterials.[6] Single-molecule detection (SMD) technique is a powerful tool to investigate

nanometer-sized materials and has significantly advanced our understanding in the fields of nanoscience and nanotechnology. It also allows the elimination of ensemble average within heterogeneous samples. To the best of our knowledge, there are at least 5% distribution of sizes and shape for nanomaterials even by the best synthesized methods. Therefore, based on SMD technique, it can provide useful and wealthy information, such as dynamical fluctuation, diffusion, and conformational changes for a specific nanotarget. However, the spatial resolution for optical measurements is limited by the wavelength of light. For biological imaging and sensing, the usual way is to attach a label to the target of interest. The ideal labels must fulfill some requirements, which is depicted as follows: (1) the size is smaller than target, it implied that when you are interested in nanometer-sized biological systems (DNA, protein), the sizes of the markers should be down to ~nanometer range, (2) it can generate intense optical signal (either fluorescence or scattering light), (3) nonblinking and nonbleaching are necessary for long-term observation, (4) it can exhibit excellent spectral properties (wide absorption band and narrow emission band), (5) nontoxic to cells. Recently, several kinds of optical labels with nanometer sizes have been used to attach to specific biological molecules, such as organic fluorophores, semiconductor colloidal QDs,[7] noble-metal nanoparticles,[8] and nanoclusters.[9]

For semiconductor colloidal CdSe QDs, they have recently been used as fluorescent markers and sensors due to excellent fluorescence properties, including high fluorescence quantum yields (QYs, ~50%), broad absorption spectrum, narrow size-dependent emission spectrum, and better photostability. Quantum confinement of both electron and hole in all spatial dimensions leads to increase the effective band gap with decreasing the QD sizes. Colloidal QDs with different sizes can be excited by the same laser and distinguished by their specific emission spectra. However,

single-QD complex blinking behavior and toxic Cd ion are the main drawbacks for practical use. Therefore, understanding and suppression of blinking behavior are relevant for realization of single-QD applications.

For noble-metal nanoparticles (with relatively larger sizes of 10~100 nm), the most important optical feature is the localized particle plasmon resonance (LPPR).[10] In general, no fluorescence can be found in metal NPs, thus they are commonly characterized by optical Rayleigh scattering. Based on Mie's theory, the scattering cross-section of a spherical particle with radius R much smaller than the wavelength of the light, varies as R^6, while its absorption cross-section varies as R^3 only. Therefore, for very small particles (<10 nm), absorption dominates scattering, and absorption related detection methods are more sensitive. Moreover, the scattering signal must be discriminated from a strong background, especially if the particles are placed in cells.

For fluorescent gold nanoclusters (also known as nanodots), they consist of a few atoms and exhibit some advantages for applications in biological markers, including nontoxic and extremely small sizes. In fact, fluorescence from noble-metal bulk materials have been discovered for more than 30 years.[11] However, it was not attracted much attention due to very low QYs of ~10^{-10}. The low QYs are likely attributed to nonradiative energy relaxation processes of very fast electron-electron scattering.[12] Recently, fluorescence with relatively high QYs (10^{-1}~10^{-4}) was observed in relatively small nanoparticles (1~10 nm) and nanoclusters (< 1 nm).[13~14] The research in this field is still less than colloidal QDs and metal NPs. Low QYs and poor fluorescence properties are the main issues to be understood and further improved.

References

[1] M. J. Bruchez, M. Moronne, P. Gin, S. Weiss, A. P. Alivisatos, Science 281, 2013 (1998).

[2] W. C. W. Chan and S. M. Nie, Science 281, 2016 (1998).

[3] C. Y. Zhang, H. C. Yeh, M. T. Kuroki, T. H. Wang, Nature 4, 826 (2005).

[4] I. L. Medintz, A. R. Clapp, H. Mattoussi, E. R. Goldman, B. Fisher and J. M. Mauro, Nature Materials, 2, 630 (2003).

[5] A. H. Mueller, M. A. Petruska, M. Achermann, D. J. Werder, E. A. Akhadov, D. D. Koleske, M. A. Hoffbauer, and V. I. Klimov, Nano Letters 5, 1039 (2005).

[6] S. Weiss, Science 283, 1676 (1999).

[7] M. Y. Han, X. H. Gao, J. Z, Su and S. Nie, Nature Biotechnology 19, 631 (2001).

[8] N. J. Durr, T. Larson, D. K. Smith, B. A. Korgel, K. Sokolov, and A. B. Yakar, Nano Letters 7, 941 (2007).

[9] R. C. Triulzi, M. Micic, S. Giordani, M. Serry, W. A. Chiou, W. A. R. M. Leblanc, Chemical Communication 48, 5068 (2006).

[10] S. Eustis and M. A. El-sayed, Chemical Society Review 35, 209 (2006).

[11] A. Mooradian, Phys. Rev. Lett. 22, 185 (1969).

[12] E. Dulkeith et al, Phys. Rev. B 70, 205424 (2004).

Chapter 2: Introduction to Colloidal Quantum Dots

2.1 Fluorescence properties of ensemble colloidal CdSe QDs

I. Introduction

Recently, colloidal quantum dots (QDs, also known as semiconductor nanocrystals) have attracted much attention due to excellent fluorescence properties over organic dye molecules for potential applications in biological markers,[1-4] solar cells,[5] and light-emitting diodes.[6] They bridge the gap between molecule clusters and bulk materials. Colloidal QDs commonly consist of an inorganic core and shell (CdSe/ZnS, CdTe/ZnS) with an organic surfactant for synthesis (TOPO, TOP), water solubility (MPA), and biocompatibility. The main function of inorganic capping shell (ZnS) is to passivate the surface dangling bonds or defect states and thus can improve the fluorescence quantum yields to ~50%. These kinds of materials with nanometer-sized range are smaller than the bulk exciton Bohr radius (~11 nm in diameter for CdSe bulk), and exhibit strong quantum confinement effects. By using this effect, it is possible to tune the energy band gap by more than 1 eV. Therefore, the emission color can be changed over the whole visible range by varying the QD size, as shown in Fig. 2.1. Some advantages on photophysical properties were found for CdSe QDs, compared to conventional organic fluorophores. As can be seen clearly in Fig. 2.2, emission spectrum was distinct between rhodamine 6G and CdSe QDs. The QD emission spectrum is symmetric in line shape and narrow in peak width. Its absorption spectrum is broad and continuous. Furthermore, the ability of resistance to photobleaching (photostability) is much better (more than ~100 times stable than rhodamine 6G), thus are expected to be used as biological markers for long-term observations.[2]

II. Summary of advantages for colloidal CdSe/ZnS QDs

(1) Chemically synthesized QDs exhibit bright fluorescence with QYs of ~50 %.

(2) The emission colors can be tailored to cover whole visible range by varying QD sizes.

(3) The ability of resistance to photobleaching (photostability) is much better than conventional dye molecules.

(4) The spectral properties exhibit broad absorption and narrow emission band.

2.2 Band edge exciton fine structures in colloidal CdSe QDs

Band edge exciton fine structures in CdSe colloidal QDs have been calculated by Efros et al, based on effective mass approximation.[7] The asymmetric crystal field induced by Wurtzite structure splits the lowest exciton state ($1S_{1/2(e)}1S_{2/3(h)}$) into two-fold degenerate states. Incorporating crystal shape anisotropy with electron-hole exchange interaction, the band edge exciton states can be further split into five-fold degenerate states within ~20 meV for a 3 nm QD, as illustrated in Figure 2.3. These discrete energy levels are denoted by their total angular momentum projection along the c axis, $F_m = m_e + m_j$, where $m_{e(j)}$ is the electron (hole) angular momentum projection. U and L denote the upper and lower states with the same angular momentum and the dotted lines denote optically spin forbidden states (so-called dark exciton states). Note that the lowest exciton state is a dark exciton state and the lowest bright exciton states lies slightly above dark exciton states (~1 to 10 meV depending on QD sizes). This dark exciton states have been evidenced by observing unusually long radiative lifetime of ~ 1 μs at 10 K.[8]

2.3 Single-molecule detection

I. Background

An important progress for nanoscience was the invention of single-molecule detection (SMD) techniques to investigate the nanomaterials down to only one nano-object at the same time.[9,10] Recently, individual nano-objects can be probed either by optical microscopy (confocal microscopy or total internal reflection microscopy), as shown in Fig. 2.4 or scanning probe microscopy if the samples were located onto the surface. The advantage of optical microscopy on transparent materials is that it is not limited to surfaces. Because of no requirement of direct contact to the samples, SMD technique based on optical microscopy is a non-invasive method to study single-isolated nano-objects. Moreover, this technique can also provide dynamic information for individual nano-objects, for example, fluorescence time trajectories, real time fluorescence resonance energy transfer measurements, temporal fluorescence lifetime. These functions can not be replaced by scanning probe microscopy. However, the spatial resolution for optical microscopy is restricted by optical diffraction limit. In general, individual nano-objects even from the same batch can distribute somewhat heterogeneity (such as, size, shape, and surface). Therefore, ensemble measurements can only reflect average behavior and hide some interesting properties that only exhibit at a single-particle level, such as fluorescence intermittency,[11] fluorescence spectra diffusion,[12] and fluorescence lifetime fluctuations.[13]

II. Summary of advantages for single-molecule detection

(1) Heterogeneity can be suppressed. Nanometer-sized samples with distributions of at least 5% in size, shape, and local nanoenvironment always occurred regardless of various preparation methods.

(2) Time-dependent fluctuations (real-time observation) can be directly reflected without any requirement of synchronization. Conventional ensemble measurements can only exhibit average behavior and blind to fluctuations unless synchronization.

(3) Applications in ultra-sensitive nano-biosensor. By using this technique, one can probe the local properties of specific interested nano-target, for example protein folding/unfolding dynamics.

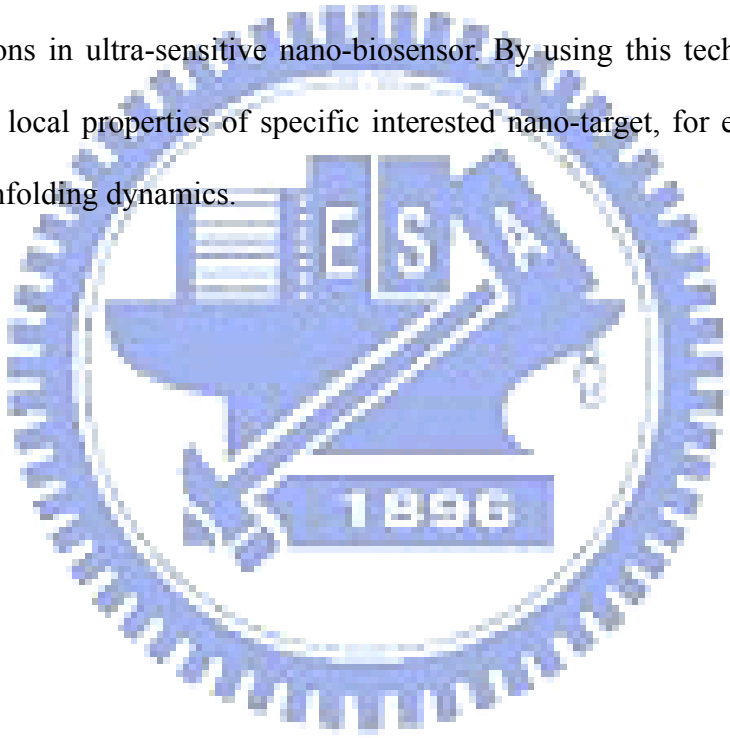

2.4 Single-QD fluorescence blinking

I. Introduction to fluorescence blinking

Fluorescence intensity from a single nano-object is not constant, but reveals abrupt fluctuation with time, usually called fluorescence intermittency or blinking.[11] This phenomenon can be reflected on the fluorescence time traces (fluorescence intensity as a function of observation time), which exhibits alternative on and off-states (finite periods of laser induced fluorescence and finite periods of darkness), but average out for ensemble measurements, as shown in Fig. 2.5 Therefore, this characteristic can be used as a criteria for emission of single nano-objects. Blinking behavior has been observed extensively, for example, colloidal semiconductor QDs,[11] self-assembled QDs,[14] Si nanocrystals,[15] noble-metal nanoparticles,[16] and fluorescence protein.[17] Recently, the fluorescence blinking from single colloidal QDs has attracted much attention due to relatively long observation time of fluorescence time traces (in general, $>10^8$ emitted photons for a given single colloidal QDs, compared to single molecule of 10^6 emitted photons due to fast photobleaching). From statistical analysis of fluorescence time traces for ZnS capped CdSe QDs, sufficient data (seven decades in probability density and five decades in times) can be extracted to construct the distributions of on/off-times.[18] However, the underlying mechanism for fluorescence blinking is still under debate. The statistics of fluorescence blinking behavior has revealed many interesting dynamics, such as, universal power-law distributions for both on and off-times,[19] and enhanced fluorescence blinking.[20] The timescales of blinking events in the range between milliseconds and minutes, longer than those of intrinsic quantum dynamics (~nanoseconds).

II. Universal power-law distribution

At first insight, blinking behavior seems to exhibit random distribution. However, when the histograms (or probability) of on/off-times were statistically constructed, the universal power-law distribution ($P(\tau) \propto \tau^{-\alpha}$) can be found, as shown in Fig. 2.6 This power-law distribution can extend to many decades of times and its exponent has been found only in the range between 1.1 and 2.2. This value slightly depends on the predefined intensity threshold and bin time. In general, power-law behavior extends over a larger range for off-times than on-times.[21] For high excitation power regime, the on-time distribution is slightly deviated from power-law for relatively long on-time and can be described by a exponential cutoff.[21] The off-time distribution exhibits independent of temperature and excitation intensity.

III. Analysis of blinking statistics

The general way to analyze the blinking statistics from fluorescence time traces is to set a proper threshold intensity to distinguish between on/off-times. This threshold intensity is defined by measuring the background fluorescence intensity in the dark area (i.e. areas with no QDs) as reference. By setting this intensity threshold, the events of on/off-time length were determined and can be used to construct the histogram, as shown in Fig. 2.6. In general, both the histograms of on/off-times exhibit universal power-law distributions (i.e. the linear relationship between on/off-time events and on/off-time lengths by a log-log plot). A parameter called probability density defined as $P(\tau_{on/off}) = \frac{N(\tau_{on/off})}{N_{on/off}^{total}}$ can be determined. According to this equation, the probability density for any $\tau_{on/off}$ occurring only once is the same, and for any $\tau_{on/off}$ not happened is zero. Thus, power-law behavior can be deviated for relatively long on/off-time range due to rare events (poor statistics), as can be seen in Fig. 2.6. Therefore, a much longer experiment with more events needs to perform to gain a different probability for these rare events. Unfortunately, photoinduced sample bleaching as well as time wasting, and long-term mechanical drift of objective, are the main obstacles to perform the long-term experiment. To solve this problem, Kuno et al,[18] proposed a weighted probability density as $P(\tau_{on/off}) = \frac{N(\tau_{on/off})}{N_{on/off}^{total}} \times \frac{1}{\Delta t_{on/off}^{average}}$, here $\Delta t_{on/off}^{average} = \frac{(a+b)}{2}$, where a, b are the time differences between the next longest and next shortest observed events. Based on this method, smooth relationship can be obtained.

IV. Features of blinking behavior

(1) It was observed for many various species of single emitters and for different chemical compositions within each class.

(2) The power-law behavior extends to many decades for both time and probability density.

(3) The power-law exponent is in the range between 1.1 and 2.2 for either on-times or off-times.

(4) The power-law exponent for on-time is usually larger than off-times.

(5) A deviation from a power-law (exponential cutoff) was found for relatively long on-times.

(6) The off-time exponent is insensitive to temperature and excitation power.

(7) The surfactant molecules and surrounding environments can influence the blinking behavior.

(8) Some phenomena occurred with fluorescence blinking, such as lifetime fluctuations and spectra diffusion.

V. Models for fluorescence blinking

It is generally accepted that fluorescence blinking in colloidal CdSe QDs is attributed to alternative ionization/neutralization of QDs due to photogenerated carriers transfer between QDs and QD surface/interface or surrounding matrix.[11] This carrier is likely an electron instead of a hole because of its smaller effective mass. This charge transfer behavior has been demonstrated by means of electric force microscopy.[22~25] The most promising feature is the universal Power-law distributions for both on/off-times and wide range blinking rates (10^{-4}~10^{2} Hz). The crucial issues for blinking mechanism are how the carrier is ejected from a QDs and returned back, thus caused power-law distributions with wide rang blinking rates. Therefore, the models should be consistent with experimental observations (wide range blinking timescales from milliseconds to minutes, and power-law distributions for on/off-times).

(a) Photoinduced ionization by Auger process

The first proposed theoretical model for single-QD blinking phenomenon is a photoinduced ionization models.[26] This model is depicted in Fig. 2.7. For nanometer-sized colloidal QDs, there is a finite possibility to generate two electron-hole pairs simultaneously under above band gap excitation. In this case, efficient nonradiative Auger process (~ps, depends on QD sizes) prevails the radiative recombination (~20 ns).[27] It means that one electron-hole pair can recombine nonradiatively and then transfer their energy to remaining electrons. Subsequently, this electron can obtain enough energy to escape from QDs to trap states located either on the surface or in the surrounding matrix. Therefore, charged QDs can be formed by photoinduced ionization process. Charged QDs can still absorb excitation photons but fluorescence was significantly quenched by efficient Auger process due to excess charges, referred to as off-times (off states). Neutralization of the charged QDs will restore the fluorescence cycles. Based on this model, fluorescence blinking on-times are inversely proportional to the excitation intensity, but off-times are insensitive to excitation power. This ionization/neutralization can be further verified by comparing the QDs with/without ZnS shell, as shown in Fig. 2.8. Obviously, fluorescence time traces for ZnS capped QDs, on/off-times were both increased and resulted in the reduction of blinking rates. It indicates that role of ZnS is as a barrier to ionization and potentially passivate interface/surface trap states. However, based on this model, it is difficult to explain the extremely wide on-time range (~ms to min) and universal power-law distribution. If the transition between on and off states occurred only via photoinduced ionization process, the transition rate is proportional to double electron-hole pair formation. For a constant excitation power and constant absorption cross-section, a two-photon absorption rate should be a constant, and thus lead to a single exponential distribution for on-time duration. Efros et al,[26] have

theoretically modeled this blinking behavior by photoinduced ionization process. They found that the distributions for on/off-times both exhibit a single exponential distribution. This is inconsistent with experimental observations (power-law distribution).

(b) Thermal activated models

Another route to eject electron from the QD core is a thermally activated process.[28] Some experimental observations support this thermal trapping models, such as (1) the number of on/off cycles is dramatically decreased at low temperature. (2) on-times exhibit Arrhenius activated behavior. For photoinduced ionization process, it can provide enough energy to eject electron over the large barrier into high energy trap states in the surrounding matrix. However, thermal ionization should result in charge trapping onto different sites. The energy position for these trap sites should lie within the ~kT of conduction bands.

(c) Tunneling models

Direct tunneling from QD core to the surrounding substrate for excited electron is another way to cause ionized QDs.[18,19] Tunneling was evidenced by the observations of redshift both in absorption and fluorescence spectrum upon capping additional ZnS thin layers.[29] In this models, it is necessary to introduce external trap states outside the QDs to generate sufficiently long on/off-times on the timescales of the experiments. The ionized rate depends on tunneling barrier height and width. For simplicity, one-dimension tunneling model can be used to describe this behavior, $\gamma_{tunnel} = A\exp(-\sqrt{\frac{8m\Delta E}{\hbar^2}}l)$, where ΔE and l are the barrier height and width, respectively. According to tunneling models, the ranges of blinking rates can be

spread from 10^{4} to 10^{-2} Hz (0.1 ms to 100 s) corresponding to tunneling distance from ~1 to ~2 nm.[30] This indicated that outside trap states are required for tunneling models.

(d) Diffusion-controlled models

A diffusion-controlled model was proposed by Shimizu et al,[21] who suggested that the trap state energy undergoes a random walk. When the energy between QD excited states and trap states are in resonance, charge carriers can transfer between QDs and trap states. In this model, trap state is assigned to dark-state, and QD state is on-state. Therefore, the duration of on/off-time depends on the time that the trap states diffusion in or out-of resonance conditions. This diffusion-controlled electron transfer model was further developed by Tang and Marcus.[31~32]

2.5 Fluorescence dynamics of single QDs

Time-resolved fluorescence spectroscopy is a complementary technique to study the fluorescence properties. Combining fluorescence time traces and decay dynamics, we can obtain more insight into fluorescence behavior.[13] Comparison with conventional organic chromophores, the striking differences in decay dynamics for ensemble colloidal QDs are as follows: (1) Relatively long lifetimes are observed (~20 ns at room temperature to ~ms at low temperature). (2) the decay profiles exhibit universal multi-exponential dynamics. Some possible explanations for multi-exponential dynamics in ensemble colloidal QDs are as follow:[33] (1) each single QD within ensembles has its single lifetime, however, average behavior deviate from pure single-exponential dynamics due to the distribution of size, shape, and local environments, (2) the fluorescence decay dynamic even for single QDs itself is a complex process, (3) the decay dynamics is single-exponential for a given moment, but it fluctuates with time, thus time-averaged decay of a single QD is multi-exponential.

Figure 2.9 (a) shows the fluorescence time traces for a single CdSe/ZnS QDs accompanied with fluorescence decay profile (b), which collects all photons for 100 s integration time. Obviously, multi-exponential decay profile was found, even down to single-QD level. For understanding correlation between fluorescence intensity and lifetimes, time-tagged and time-resolved measurements (TTTR, detailed description in chapter 3) were measured. Based on this TTTR measurement, we can set an intensity or time gate to select a section of photons to construct lifetime decay profiles. Figure 2.9 (c) shows fluorescence decay profiles for three different intensity gates, as indicated by black-dotted line. To describe multi-exponential decay profiles, a stretched exponential decay function, $I(t) = I_0 \exp(-(\frac{t}{\tau})^{\beta})$, where $0 < \beta \leq 1$, can be

used to fit our experimental results. This function describes the decay processes with continuous decay rates, which a smaller β means a broader rate distribution. For β=1, it implied this decay profile is pure single exponential with only one decay rate.[33] Strong correlation between fluorescence intensity and lifetime can be found. Where, higher intensity corresponds to longer lifetime and with a β value more close to unity.

Figure 2.1: Emission color under UV illumination for colloidal CdSe/ZnS QDs with various sizes.

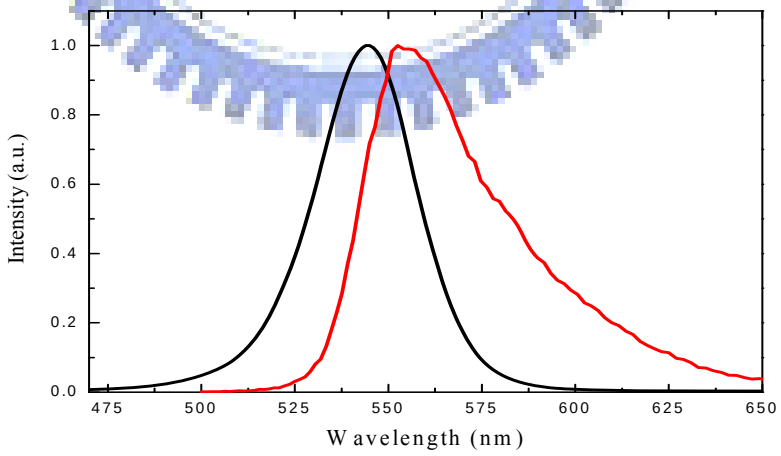

Figure 2.2: Emission spectra of R 6G (red line) and colloidal QDs (black line).

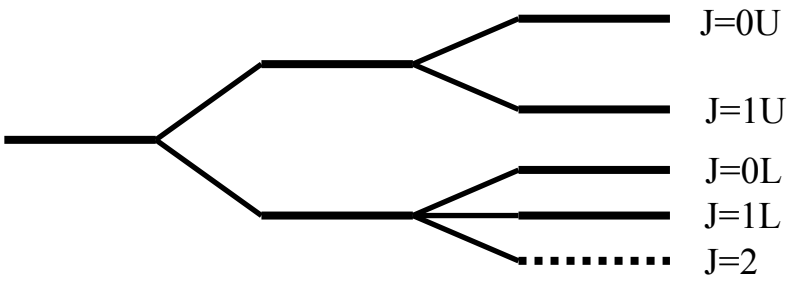

Figure 2.3: Band edge exciton fine structures in colloidal CdSe QDs.[7]

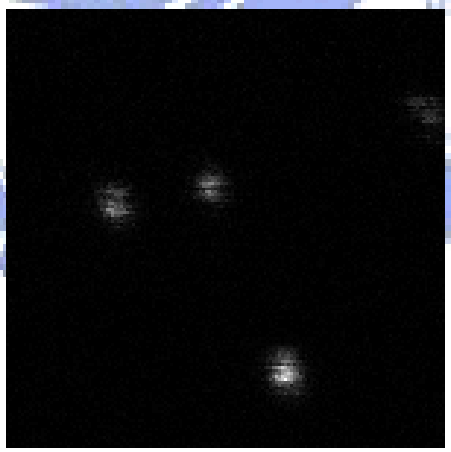

Figure 2.4: Fluorescence images with $4 \times 4 \mu m^2$ for single CdSeTe/ZnS QDs onto a glass coverslips.

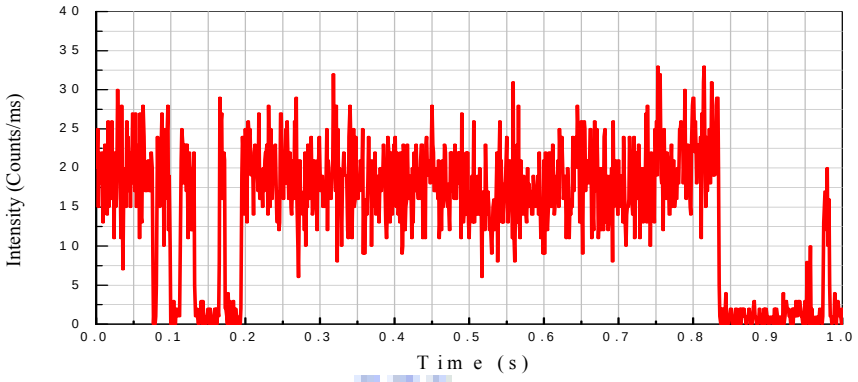

Figure 2.5: Fluorescence time traces of single colloidal CdSe/ZnS QDs.

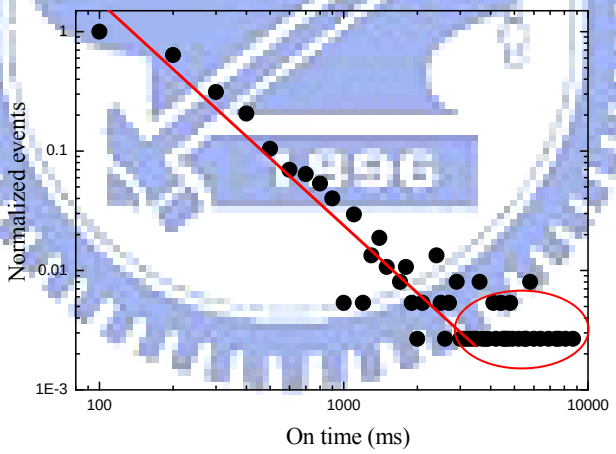

Figure 2.6: Histogram of normalized events of on-time length by log-log plot.

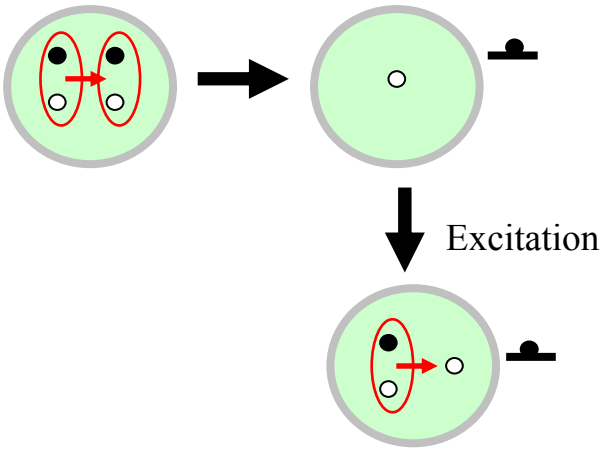

Figure 2.7: Schematic illustration of photoinduced ionization by Auger process.

(a)

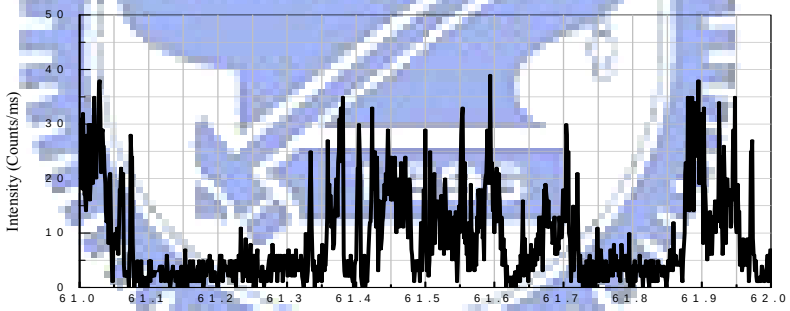

(b)

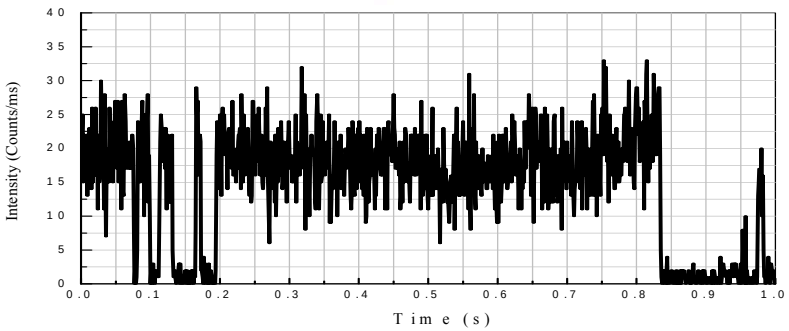

Figure 2.8: (a) Fluorescence time traces for a single bare CdSe QDs and (b) core/shell CdSe/ZnS QDs.

(a)

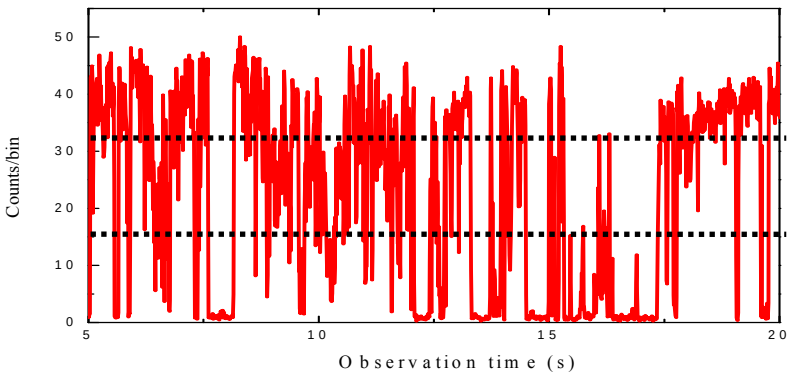

(b)

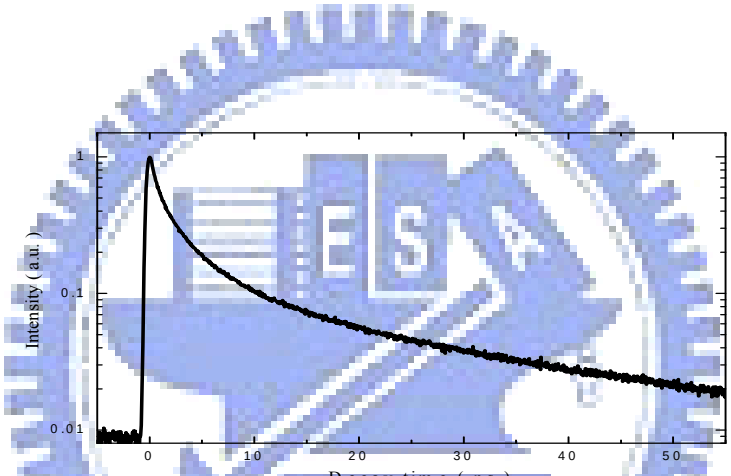

(c)

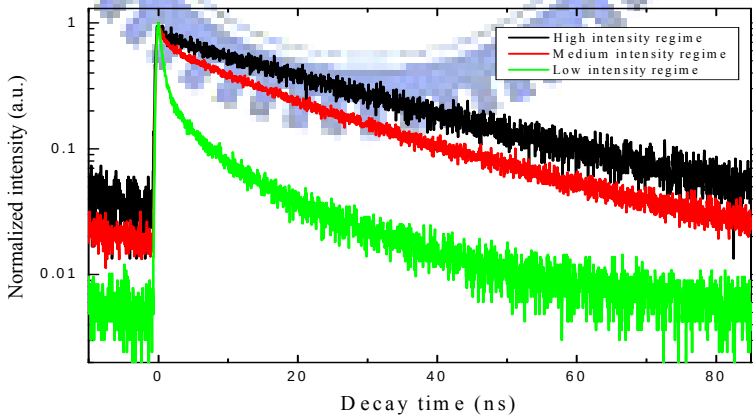

Figure 2.9: (a) Fluorescence time traces for a single CdSe/ZnS QDs accompanied with time-resolved fluorescence spectra (b), and (c) decay profiles with various intensity regimes.

References

[1] M. Bruchez Jr, M. Moronne, P. Gin, S. Weiss, A. P. Alivisatos, Science 281, 2013 (1998).

[2] W. C. W. Chan and S. Nie, Science 281, 2019 (1998).

[3] X. Michalet, F. F. Pinaud, L. A. Bentolila, J. M. Tsay, S. Doose,. J. J. Li, G. Sundaresan, A. M. Wu, S. S. Gambhir, S. Weiss, Science 307, 538 (2005).

[4] I. L. Medintz, H. T. Uyeda, E. R. Goldman, H. Mattoussi, Nature Materials 4, 435 (2005).

[5] W. U. Huynh, J. J. Dittmer, A. P. Alivisatos, Science 295, 2425 (2002).

[6] S. Coe, W. K. Woo, M. G. Bawendi, V. Bulovi, Nature 420, 800 (2002).

[7] A. L. Efros and M. Rosen, Phys. Rev. B 54, 4843 (1996).

[8] M. Nirmal, D. J. Norris, M. Kuno, M. G. Bawendi, A. L. Efros, and M. Rosen, Phys. Rev. Lett. 75, 3728 (1995).

[9] S. Weiss, Science 283, 1676 (1999).

[10] W. E. Moerner and M. Orrit, Science 283, 1670 (1999).

[11] M. Nirmal, B. O. Dabbousi, M. G. Bawendi, J. J. Macklin, J. K. Trautman, T. D. Harris, Nature 383, 802 (1996).

[12] R. G. Neuhauser, K. T. Shimizu, W. K. Woo, S. A. Empedocles, and M. G. Bawendi, Phys. Rev. Lett. 85, 3301 (2000).

[13] G. Schlegel, J. Bohnenberger, I. Potapova, A. Mews, A. Phys. Rev. Lett. 88, 137401 (2002).

[14] M. E. Pistol, P. Castrillo, D. Hessman, J. A. Prieto, and L. Samuelson, Phys. Rev. B 59, 10725 (1999).

[15] F. Cichos, J. Martin and C. V. Borczyskowski, Phys. Rev. B 70, 115314 (2004).

[16] C. D. Geddes, A. Parfenov, I. Gryczynski, and J. R. Lakowicz, J. Phys. Chem. B 107, 9989 (2003).

[17] R. M. Dickson, A. B. Cubitt, R. Y. Tsien, and W. E. Moerner, Nature 388, 355 (1997).

[18] M. Kuno, D. P. Fromm, H. F. Hamann, A. Gallagher, and D. J. Nesbitt, J. Chem. Phys. 115, 1028 (2001).

[19] M. Kuno, D. P. Fromm, H. F. Hamann, A. Gallagher, and D. J. Nesbitt, J. Chem. Phys. 112, 3117 (2000).

[20] M. Yu and A. V. Orden, Phys. Rev. Lett. 97, 237402 (2006).

[21] K. T. Shimizu, R. G. Neuhauser, C. A. Leatherdale, S. A. Empedocles, W. J. Woo, and M. G. Bawendi, Phys. Rev. B 63, 5316 (2001).

[22] T. D. Krauss and L. E. Brus, Phys. Rev. Lett., **83**, 4840 (1999).

[23] T. D. Krauss, S. O. Brien, and L. Brus, J. Phys. Chem. B **105**, 1725 (2001).

[24] O. Cherniavskaya, L. Chen, and L. Brus, J. Phys. Chem. B **108**, 4946 (2004).

[25] O. Cherniavskaya, L. Chen, M. A. Islam, and L. Brus, Nano Lett. **3**, 497 (2003).

[26] A. L. Efros, and M. Rosen, Phys. Rev. Lett. **78**, 1110 (1997).

[27] V. I. Klimov, A. A. Mikhailovsky, D. W. McBranch, C. A. Leatherdale, M. G. Bawendi, Science **287**, 1011 (2000).

[28] U. Banin, M. Bruchez, A. P. Alivisatos, T. Ha, S. Weiss, and D. S. Chemla, J. Chem. Phys. 110, 1195 (1999).

[29] B. O. Dabbousi, J. R. Viejo, F. V. Mikulec, J. R. Heine, H. Mattoussi, R. Ober, K. F. Jensen, M. G. Bawendi, *J. Phys. Chem. B* 101, 9463 (1997).

[30] M. Kuno, D. P. Fromm, S. T. Johnson, A. Gallagher, and D. J. Nesbitt, Phys. Rev. B 67, 125304 (2003).

[31] J. Tang and R. A. Marcus, Phys. Rev. Lett. 95, 107401 (2005).

[32] J. Tang and R. A. Marcus, J. Chem. Phys. 123, 054704 (2005).

[33] B. R. Fisher, H. J. Eisler, N. F. Stott, and M. C. Bawendi, J. Phys. Chem. B 108, 143 (2004).

Chapter 3: Experiments and Techniques

3.1 Laser scanning confocal microscopy

Recent developments in fluorescence microscopy have allowed for the detection, imaging, and spectroscopy of single nanometer-sized materials.[1~3] For this purpose, two main techniques, laser scanning confocal microscopy (LSCM) and wide-field microscopy (WFM) are used to achieve this work. For WFM methods, a high sensitive CCD camera is used. However, due to relatively long read-out time, it is restricted to monitor submicrosecond timescale process, such as fluorescence decay dynamics (~ns timescales). Due to larger illumination volume, autofluorescence originating from out-of focal areas reduces the resolution and image contrast. Alternatively, laser scanning confocal microscopy is a powerful tool for a wide range applications in biological and materials science for imaging thin optical section and fixed samples. This technique can provide better spatial resolution and better signal to noise ratio because of its small detection volume restricted by a confocal pinhole. Furthermore, combination with a single-photon avalanche photodiode, it can be utilized to probe temporal processes down to ~nanosecond timescales for a specific object. As shown in Fig. 3.1, single-QD image can be seen clearly by LSCM. The streaky pattern is attributed to fluorescence blinking during the course of laser scanning.

3.2 Single-QD measurements

The colloid suspension was diluted down to ~10^{-10} Molar (mole/L) concentration, and then dispersed onto a preclean substrate by spin coating with 3000 rpm for 2 min. Thus, the separation between particles can exceed the laser spot size of ~300 nm (as shown in Fig. 3.2), to insure that only one particle can be probed at the same time. Subsequently, a thin polymer layer of polymethylmethacrylate (PMMA, n=1.5) is covered for fixation and provides an interface to obtain high collection efficiency.[4] Based on this configuration, most of the light is radiated in the glass side (85%), which allows to collect 72% of the single-QD fluorescence by using oil-immersion objective (N.A.=1.4, Olympus x100 apochromatic). Single-QD measurements were performed by means of a laser scanning confocal microscope equipped with a piezo scanner with spatial resolution down to ~ nm (Micro Time 200, PicoQuant). The basic experimental setup for single-QD measurement is shown in Fig. 3.3 and depicted as follows: A pulsed diode laser at the wavelength of ~406 nm, ~50 ps pulse width is used as a excitation source. A polarization maintaining single-mode fiber guides the excitation laser light into the laser scanning confocal microscope. The exciting light with a Gaussian profile is collimated by an infinity corrected lens. The beam passes an excitation filter and is guided into double mirror steering component to align (shift and tilt) the laser beam to optical axis of the microscope objective. Here, we use an oil-immersion objective with high N.A. of 1.4 to focus excitation light and collect fluorescence signal. Figure 3.2 shows the laser focus pattern with diffraction-limited beam waist of ~300 nm. Fluorescence is collected by the same objective and passed through the dichroic mirror and backscattered laser light was filtered by a long pass filter (cutoff at 500 nm). A tube lens focuses the fluorescence into a confocal pinhole of 50 microns for rejecting out-of focus light. After a pinhole, the beam is refocused onto the active area of a single-photon avalanche diode (SPAD, Perkin Elmer). The

dark counts of this SPAD are ~250 counts/s. The SPAD outputs electrical signal of TTL pulses to TCSPC electronics (Time Harp 200, PicoQuant). For recording fluorescence intensity and lifetime images, objective scanning mode is used by mounting the objective onto a xy nanopositioning system. Integrated capacitive position sensors provide ~nanometer spatial resolution and stability in closed loop operation. Fluorescence images were recorded by raster scanning laser spot over the sample with an integration time of 0.6 ms/pixel.

3.3 TCSPC techniques and TTTR acquisition modes

In order to investigate photophysical dynamic process (~ns timescales), one need to monitor the time-dependent intensity profiles of the emitted light. The most simplest way is to record the intensity with time from a single excitation-emission cycles. However, there are some practical problems to prevent this technique. Firstly, the decay process is very fast on the timescales of ~ns. In order to recover fluorescence decay profiles of ~1 ns lifetimes, transient recorder required to sample at least 100 ps time steps. Secondly, the light signal is too weak. The solution is Time-Correlated Single Photon Counting (TCSPC) techniques. Based on the repetitive excitation source, it is possible to extend the data collection over multiple cycle, thus one can reconstruct the single cycle decay profiles, as illustrated in Fig. 3.4. TCSPC is based on the precise time registration of the emitted photons with respect to the exciting light pulses. The accurate timing is achieved by combination of time-to-amplitude converters (TAC) and analog-to-digital converter (ADC). The requirements for this TCSPC technique are as follow: (1) the probability for occurrence of a single photon emission per excitation cycle is low down to 1 % of repetition rates. For example, when the repetition rate is 10 MHz, the count rates should be down to at least ~10^5 counts/s. This limitation is mainly due to dead times of detector and electronics for ~100 ns after processing a photon event. (2) a single-photon sensitive detector is required. Single-photon avalanche photon diode can be used for ultra-low light detection (optical power < 1 pW) due to high quantum efficiency (~80 %) and low noise dark counts (~250 counts/s). The TCSPC electronic card (Time Harp 200, PicoQuant) can record digital photon events in time-tagged, time-resolved (TTTR) acquisition mode. In this mode, the relative time interval, τ_p between photon emission and latest laser pulse is recorded. Thus, the histogram of τ_p duration can

be constructed with 4096 time channels with minimum channel width of ~40 ps. Furthermore, for temporal observation (real time observation), such as fluorescence time traces and scanning image mapping, the absolute time, t_p from experimental starts to photon emission is also recorded with time resolution of ~100 ns. Therefore, based on this instrument, the time resolution of lifetime measurements as well as the instrument response function (IRF, as shown in Fig. 3.5) and continuously recording photon arrival times (dead times) are ~40 ps, ~300 ps, and ~100 ns, respectively. Fluorescence lifetime were obtained by fitting a suitable function based on χ^2 value of less than 1.2 and with a residuals trace that was symmetrical around the zero axis.

3.4 High pressure PL and Raman measurements

For room temperature PL measurements, the incident beam from Ti:sapphire laser were guided through the doubly BBO crystals as the excitation sources. The emitted light was dispersed by a spectrometer and detected by a liquid nitrogen-cooled charge coupled devices. Raman spectra were recorded by collecting scattering line in backscattering configuration. Incident beam from an argon ion laser with 514.5 nm wavelength was focused on a sample through a microscope objective. Notch filter was utilized to reject the unnecessary incident laser line. Hydrostatic high pressure surroundings were created within a 0.2 mm hole at the center of steel gaskets embedded in two diamond cells. Colloidal CdSe/ZnS QDs were dissolved into de-ionized water, which is used as a pressure transmit medium under relative high pressure. The applied high pressures were determined by monitoring the Raman shift of the ruby R1 line. Colloidal CdSe/ZnS QDs were wet chemical synthesized by conventional methods.

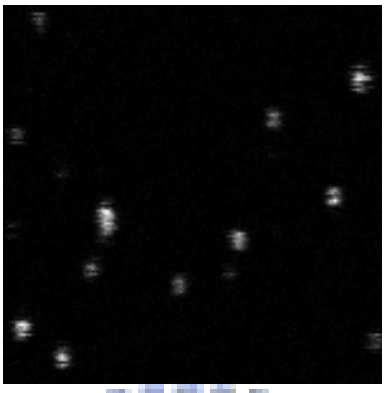

Figure 3.1: Fluorescence intensity images of $6 \times 6 \mu m^2$ for colloidal CdSe/ZnS QDs onto the glass coverslip.

Figure 3.2: Laser pattern with diffraction limited spot size of ~300 nm.

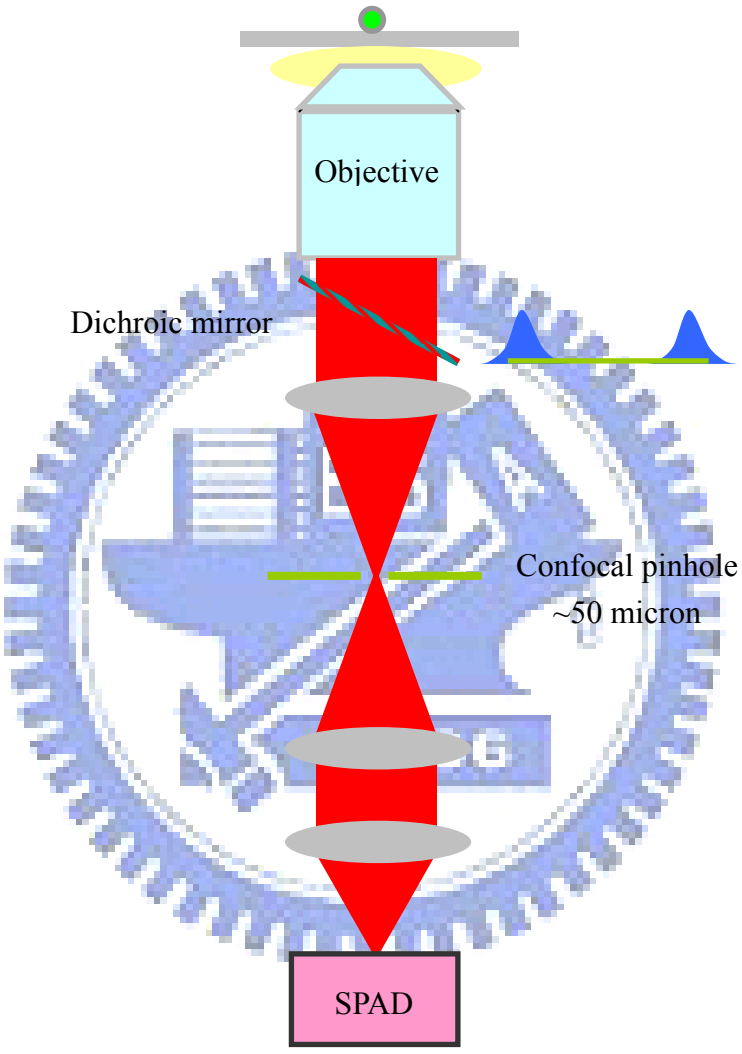

Figure 3.3: Experimental setups for single-QD fluorescence measurements.

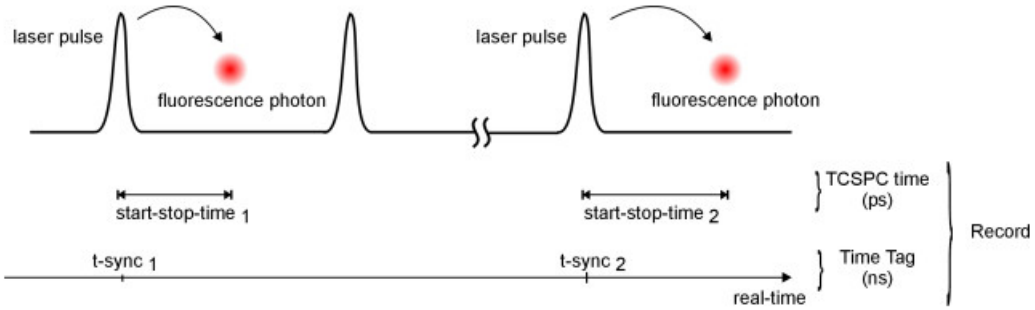

Figure 3.4: Schematic of TCSPC techniques and TTTR modes.(PicoQuant)

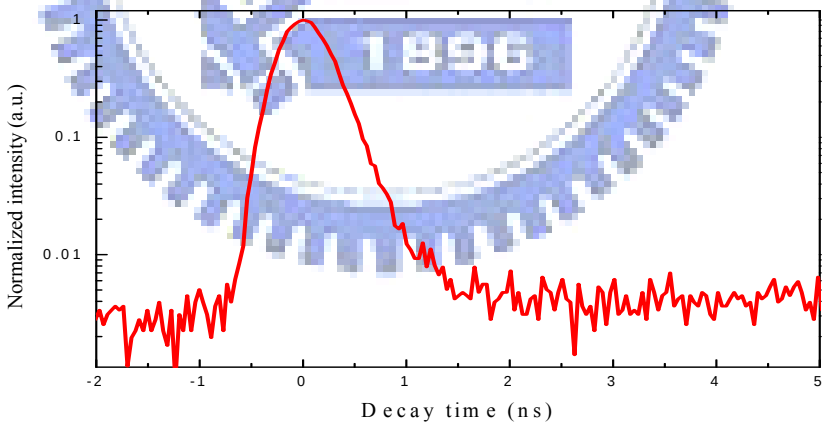

Figure 3.5: Instrument response function of experimental setup.

References

[1] E. Betzig and R. J. Chichester, Science 262, 1422 (1993).

[2] R. M. Dickson, D. J. Norris, Y. L. Tzeng, W. E. Moerner, Science 274, 966 (1996).

[3] T. Ha, T. Enderle, D. S. Chemla, P. R. Selvin, S. Wiess, Phys. Rev. Lett. 77, 3979 (1996).

[4] X. Brokmann, E. Giacobino, M. Dahan, and J. P. Hermier, Appl. Phys. Lett. 85, 712 (2004).

Chapter 4: Fluorescence Enhancement by Surface Modifications

I. Introduction

Due to high surface to volume ratio for nanometer-sized colloidal QDs, fluorescence properties are variable and sensitive to surface inorganic layer[1] and organic ligands.[2] In general, colloidal CdSe QDs with high fluorescence QYs (~50%) can be obtained by conventional hydrophobic TOP/TOPO surfactant methods. To further increase the fluorescence QYs, Talapin et al, proposed a modified method by introducing HDA (haxadecylamine) surface molecules into conventional TOP/TOPO solvent to obtain monodispersed and highly fluorescent QDs.[3] HDA ligands with high boiling points are superior agents as growth solvent for high temperature chemical synthesized methods. The mechanism of fluorescence enhancement by HDA ligands is not clear, especially from the aspect of single QDs. At the single-QD levels, the enhancement of the emission efficiency for HDA capped CdSe/ZnS QDs is attributed to the contribution of both the increase in the number of bright QDs and the enhanced intrinsic brightness of individual QDs. The former has been demonstrated by the combination of atomic force microscopy with fluorescence measurements.[4] However, the latter has not been studied in detail. An important question concerns how much of the enhancement is due to the prolongation of on-time duration and how much is related to the enhancement of QYs within the on-time duration? Therefore, in this chapter, we will investigate the fluorescence enhancement by HDA surface modifications at the single-QD level.

II. Results and discussion

Figure 4.1 shows the fluorescence spectra of ensemble colloidal CdSe QDs capped with TOPO ligands (hereafter denotes as sample a), CdSe core QDs capped with ZnS shell (sample b), and CdSe QDs capped with ZnS shell and then further modified with HDA ligands (sample c). The emission peaks of samples b and c relative to sample a are red shift due to the extension of electronic wave-function to the exterior of the QD core.[1] Additionally, the enhancement of emission intensity was observed due to the extra capping and the attachment of HDA ligands. This enhancement for ensemble QDs is generally assigned to the passivation of surface trap states around QDs.[3]

To study the origin of emission enhancement at the single-QD levels, the fluorescence from single-isolated QDs of samples a, b, and c was investigated. Figure 4.2 shows a typical fluorescence image of $6\times6\ \mu m^2$ area for sample b, CdSe/ZnS QDs. Streaky patterns with a diffraction-limited spot of ~300 nm was observed and are attributed to the fluorescence intermittency of single CdSe/ZnS QDs.[5] This characteristic is a hallmark of fluorescence emission from a single-isolated QD. In order to examine the emission behavior of a single QD, the laser spot was moved to a specific QD position to record the transient fluorescence time traces. The section of fluorescence time traces for sample a, b, and c are shown in Figure 4.3 (a), (b), and (c), respectively. For the single-QD measurements, to avoid the dot-to-dot heterogeneity, more than tens of individual QDs from the same sample were measured and averaged for comparison. The bin time (integration time) was 1 ms for the recording fluorescence time traces. These traces clearly reveal blinking phenomena, especially for sample b (CdSe/ZnS) and c (CdSe/ZnS/HDA). The dark periods are generally attributed to the formation of charged QDs by ionization processes.[5] When a charged QD absorbs a photon from the excitation laser beam, it generates a three-particle charged exciton state (neutral exciton plus one charge) within the QDs. In this case,

the fast Auger process (on the time scale of ~ps) quenches the radiative emission (on the time scale of ~ ns) through its faster energy transfer from the recombination of a neutral exciton to the charge particle.[6] As a result, the QD becomes a dark (off) state and no fluoresce can be detected. Once the charged QD is neutralized, it can emit fluorescence photon and recovers the bright (on) state.

Histograms of on-time length plotted in log-log scale are shown in Figure 4.4. The distribution follows a universal power-law behavior.[7] For comparison, the mean on-time was obtained by simple arithmetic average. We discovered that the mean on-time length can be increased to 2.3 and 5 times for sample b and c compared with sample a, but the corresponding off-time is also increased. These results can also be elucidated by the ionization model. The high band-gap ZnS capped layer blocks the ejection of electrons from (or return to) the interior QD core to (from) the outside trap states, which located either in the surrounding matrix or on the particles surface. Accordingly, the increasing on-time duration accompanied with increasing off-time. Therefore, the ratio of mean on-time to mean off-time needs to be considered to account for the emission enhancement. The on/off time ratios are almost equally for bare and ZnS capped QDs. Therefore, the fluorescence enhancement of individual QDs with ZnS shell should not originate from the increasing on/off time ratio. Interestingly, the mean on-time increased and off-time decreased for the CdSe/ZnS QDs modified by HDA ligands (sample c).

In addition to the ratio of on-time to off-time length, the number of emitted photons within the on-time duration should be taken into account to fully understand blinking behavior. In Fig.4.3, the fluorescence intensity within the on-time duration clearly varies with different surface. Histograms of the burst sizes of Fig. 4.3 are shown in Figure 4.5. The burst size is defined as the total number of emitted photons above the threshold for a given on-time duration. This burst-size can be obtained based on the

TTTR acquisition modes.[8] From the burst-size histogram, the number of bursts and mean burst-sizes can be yielded. The burst number is related to blinking rate and the burst-sizes are dependent on the on-time duration and QYs within the on-time duration. The mean burst-sizes can be enhanced up to 13-fold and accompany with a suppression of the blinking rate down to 18% by the attachment of HDA ligands to CdSe/ZnS QDs.

Subsequently, we would like to discuss the possible role of HDA ligands in fluorescence enhancement. Here, we mainly concentrate on the alteration of the blinking behavior induced by capping additional HDA ligands for individual CdSe/ZnS QDs. HDA are superior agents as coordinating solvent for high temperature organo-metallic synthesized methods because of its high boiling points. In addition, the less steric occupation than TOPO caused the high degree of surface passivation. After capping with HDA ligands (compared with sample b and c), three considerable modifications in blinking behavior was found, extension of on-time length, enhancement of fluorescence intensity within the on-time duration, and shortening of off-time length. According to ionization model, on-time can be ceased upon ejecting photo-generated electron from QD core to outside trap states located either in the surrounding matrix or on the particle surface, and recovers once the ejected electron returns to QDs. Therefore, for both extension of on-time length and enhancement of fluorescence intensity can be explained by higher degree of surface passivation. This led to reduce surface states around the particle surface, which, act as the role of trapping photo-generated electrons. It can also be proved by time-resolved fluorescence measurements of single QDs (next paragraph). For shortening of off-time length, we suggest that the HDA ligands could act as electron donors to donate electron to neutralize the charged QDs.[9] This overall contribution caused burst-sizes to enhance up to 13-fold for HDA capped CdSe/ZnS QDs.

To verify the above suggestions, time-resolved fluorescence measurements were performed to monitor the photo-excited carrier dynamics of single QDs. Figure 4.6 (a), (b) and (c) reveals the fluorescence decay profiles for samples a, b, and c, respectively. All decay profiles exhibit universally non-exponential behavior, but has different average lifetime. We also found that the decay profile of ZnS/HDA capped QDs is most close to a single exponential curve with longest lifetime. Reasonable reasons are as follow. Previous report demonstrated that the measured lifetimes vary with time due to fluctuation of non-radiative decay rates, but strongly correlate with the fluorescence intensity.[10] (i.e. strong fluorescence intensity is associated with longer lifetime). The measured decay rates are the sums of radiative and nonradiative decay rates. In general, the radiative process is not affected by the surface capping and only the nonradiative decay channels can be modified. For ZnS/HDA capped QDs, the nonradiative decay channel can be suppressed by the high degree passivation of surface trap states. Thus, the fluorescence intensity and measured lifetimes increased. Furthermore, a stretched exponential function $I(t) = I_0 \exp\left\{-(\frac{t}{\tau})^{\beta}\right\}$ is fitted to the experimental data. This equation is usually used to describe a decay process with non-separable superposition decay rates. Where τ is a mean lifetime constants and $0 < \beta \leq 1$ is a stretched dispersion parameter, which represents the degree of spread of lifetime distribution. For β=1, the fluorescence decay curve exhibits a pure single exponential profile with the narrowest lifetime distribution, which means radiative processes dominate. For ZnS/HDA capped QDs, it has the longest lifetime and largest β value. These results can also be reflected on the distribution of lifetime. Figure 4.7 is the probability of occurrence of lifetime, which can be obtained by using so called Maximum Likelihood Estimator fitting methods for every 200 ms during whole fluorescence measurements.[11] We also found that ZnS/HDA capped QDs has

narrowest lifetime distribution, which is consistent with largest β value. It implies that non-radiative decay channels can be suppressed by the high degree passivation of surface trap states.

III. Conclusions

Fluorescence of CdSe/ZnS QDs has been investigated at the single QD level and is shown that it can be enhanced by the attachment of HDA ligands. The blinking behavior of individual CdSe/ZnS QDs can be dramatically modified by additional HDA ligands. The on/off time ratio and the total number of emitted photons within the on-time duration can be enhanced up to 2.8 and 13-fold, respectively. Consequently, the blinking rate can be suppressed down to 18%. The fluorescence decay curve exhibits more close to single exponential decay profile and has longer measured lifetime. These results suggested that HDA ligands can provide the higher degree of surface passivation.

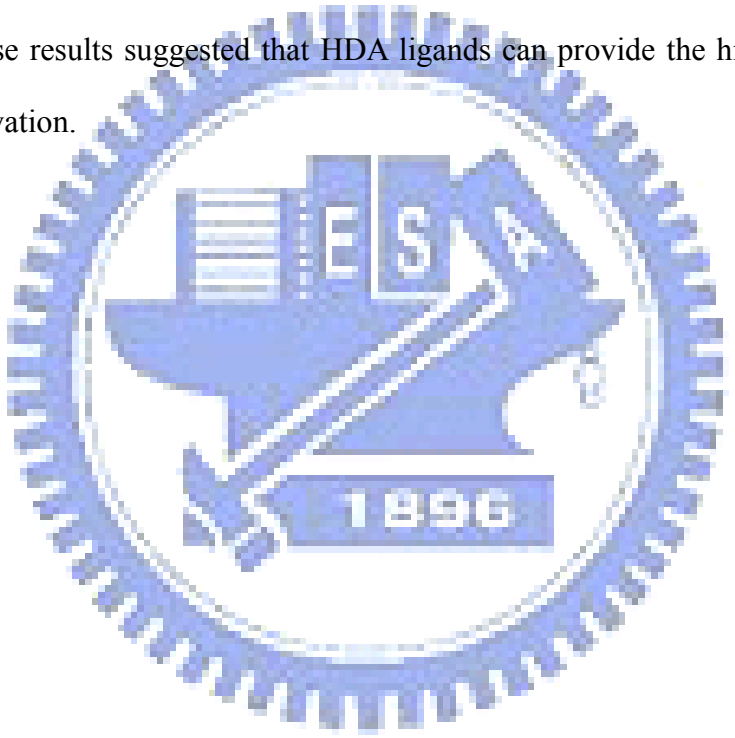

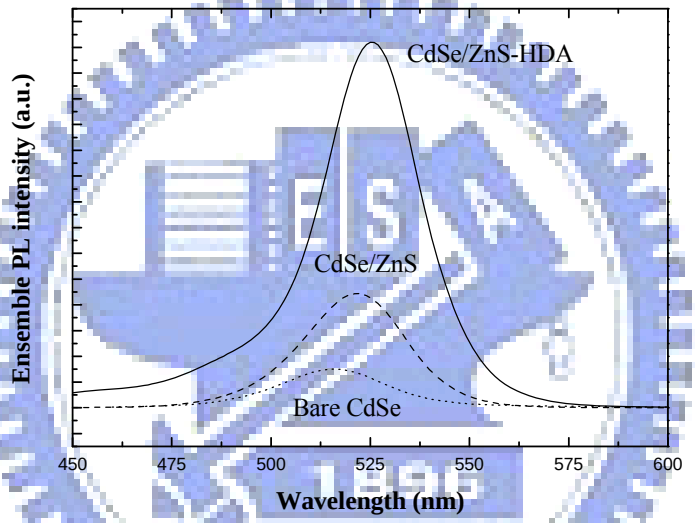

Figure 4.1: Fluorescence spectra of ensemble colloidal CdSe QDs with TOPO, ZnS shell, and ZnS/HDA surfaces.

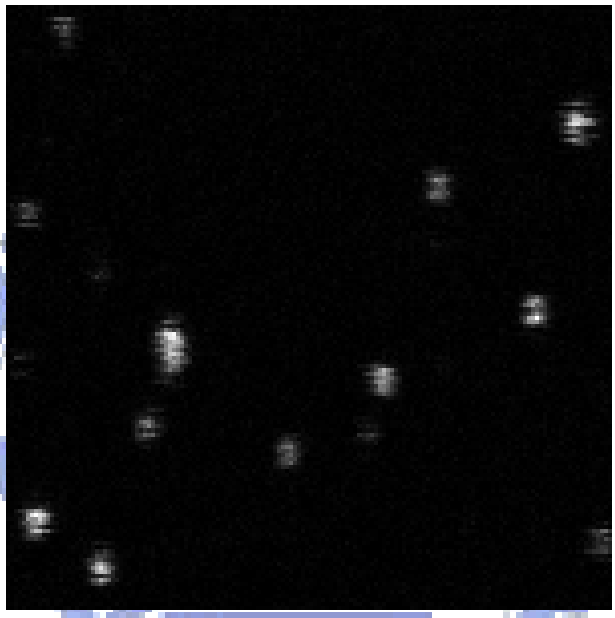

Figure 4.2: Fluorescence intensity images of $6\times6\ \mu m^2$ area from single colloidal CdSe/ZnS QDs.

(a)

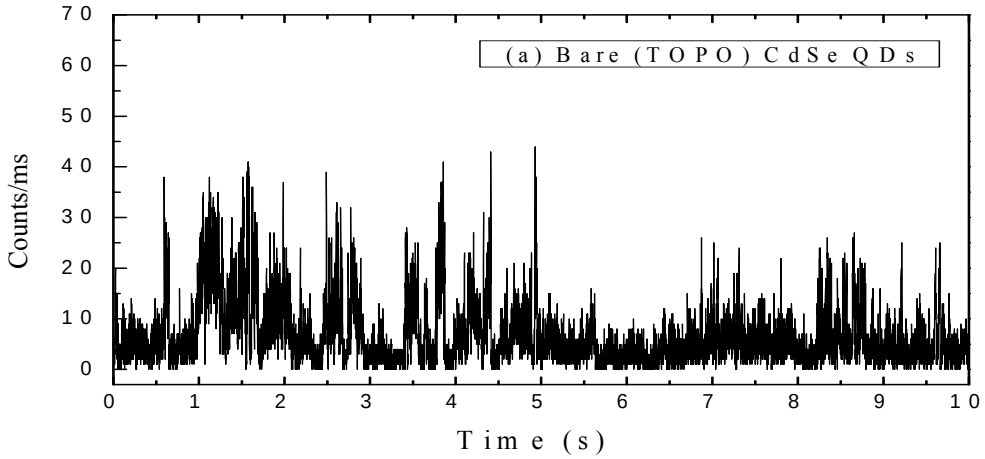

(b)

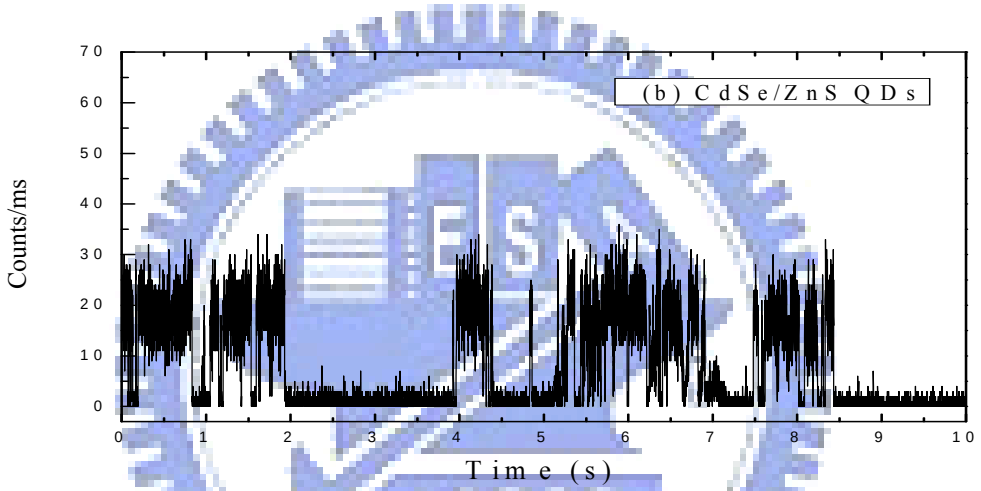

(c)

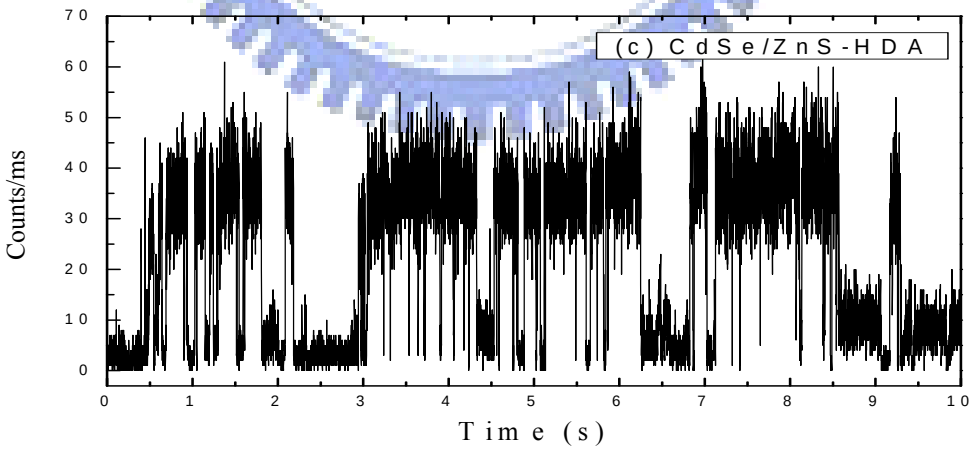

Figure 4.3: Fluorescence intensity time traces for CdSe QDs with (a) original TOPO, (b) ZnS shell, and (c) ZnS/HDA.

(a)

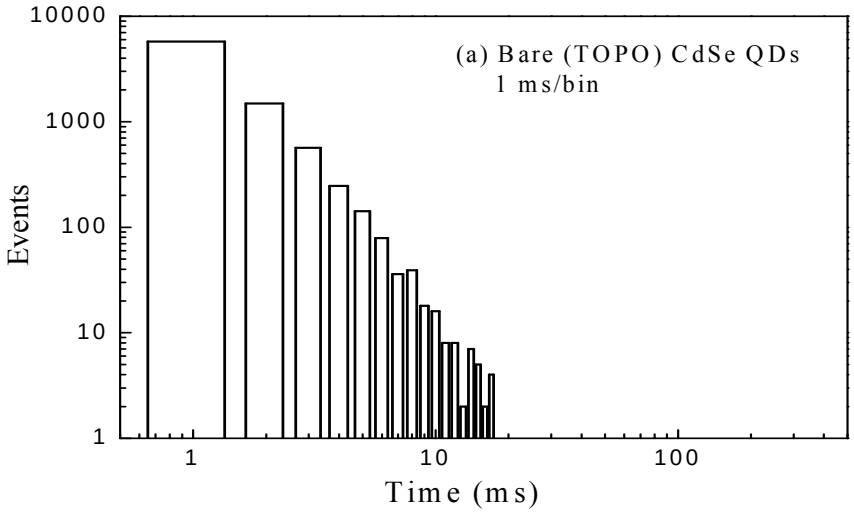

(b)

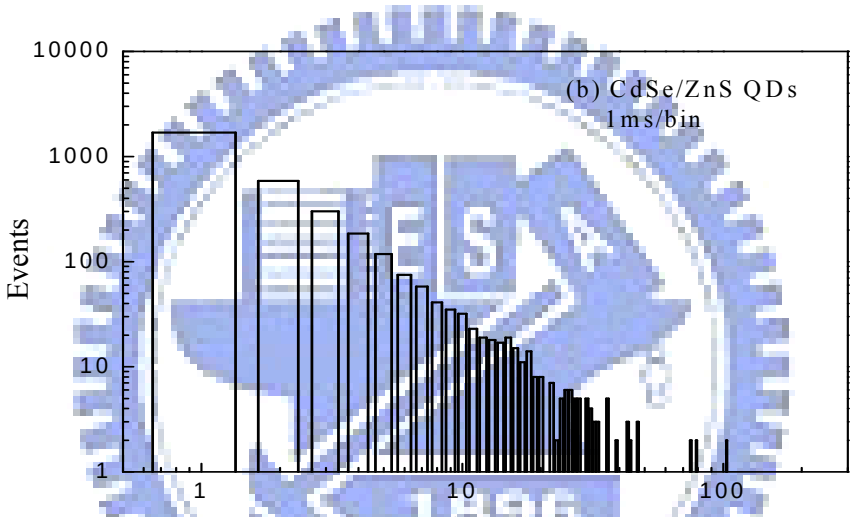

(c)

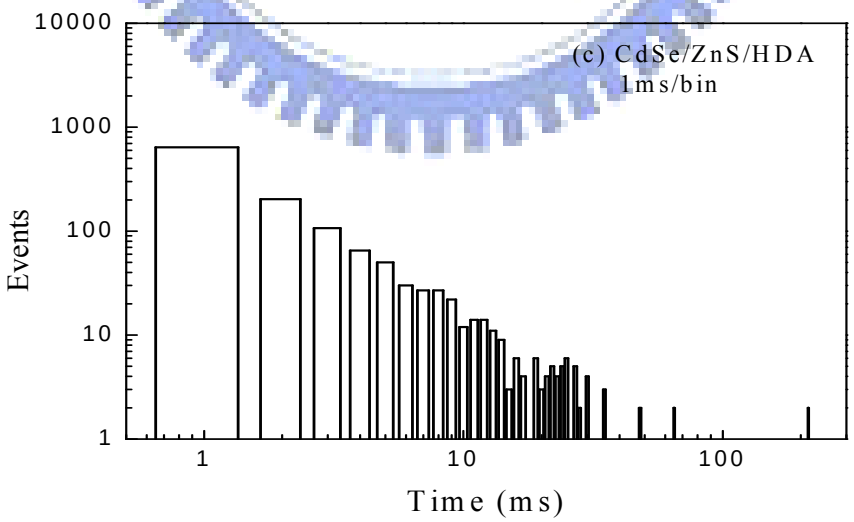

Figure 4.4: Histograms of on-time duration for CdSe QDs with (a) original TOPO, (b) ZnS shell, and (c) ZnS/HDA.

(a)

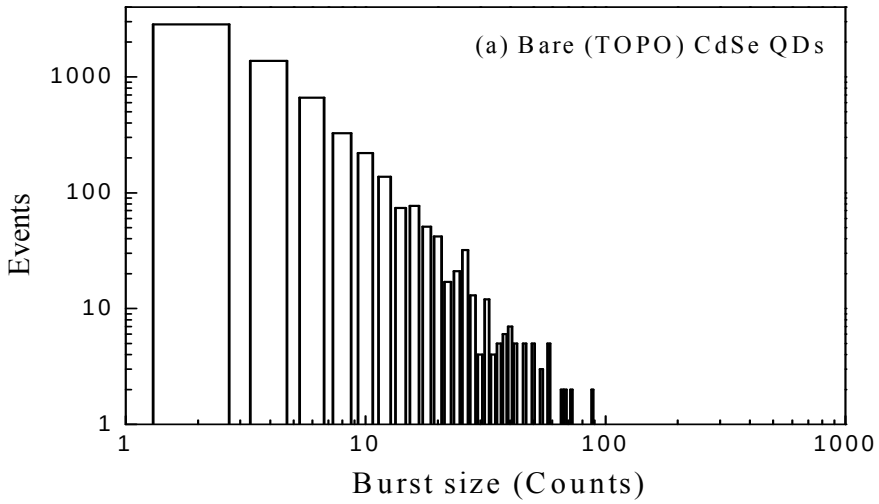

(b)

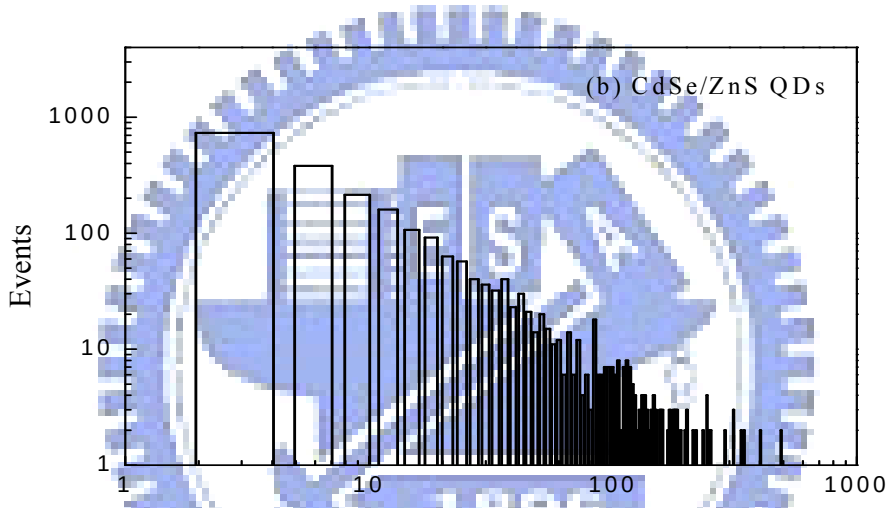

(c)

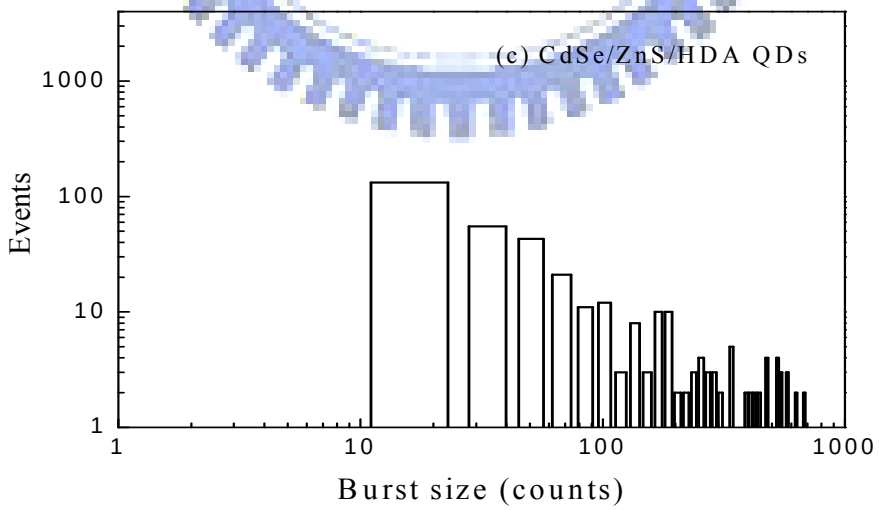

Figure 4.5: Histograms of burst sizes for CdSe QDs with (a) original TOPO, (b) ZnS shell, and (c) ZnS/HDA.

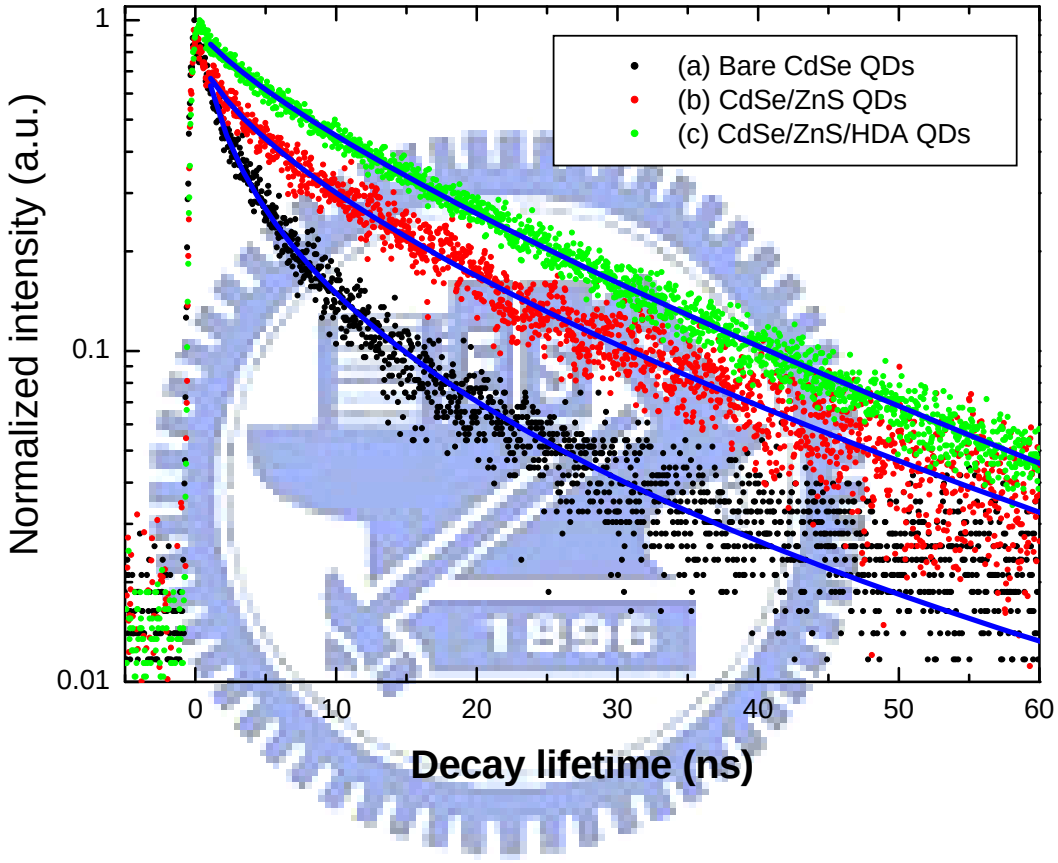

Figure 4.6: Fluorescence decay profiles for CdSe QDs with (a) original TOPO, (b) ZnS shell, and (c) ZnS/HDA.

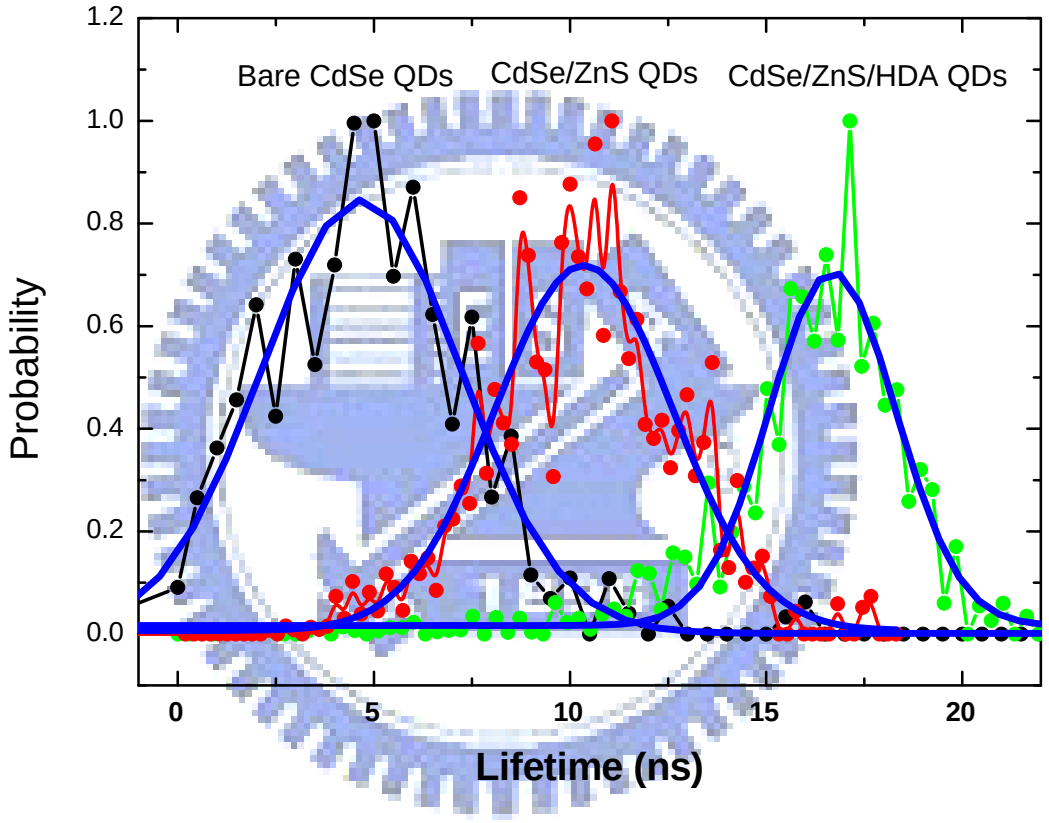

Figure 4.7: Distribution of fluorescence lifetime for CdSe QDs with original TOPO, ZnS shell, and ZnS/HDA.

Reference

[1] B. O. Dabbousi, J. R. Viejo, F. V. Mikulec, J. R. Heine, H. Mattoussi, R. Ober, K. F. Jensen, M. G. Bawendi, J. Phys. Chem. B 101, 9463 (1997).

[2] J. A. Kloeeptr, S. E. Bradforth, J. L. Nadean, J. Phys. Chem. B 109, 9996 (2005).

[3] D. V. Talapin, A. L. Rogach, A. Kornowski, M. Haase, H. Weller, Nano Letter 1, 207 (2001).

[4] Y. Ebenstein, T. Mokari, U. Banin, Appl. Phys. Lett. 80, 4033 (2002).

[5] M. Nirmal, B. O. Dabbousi, M. G. Bawendi, J. J. Macklin, J. K. Trautman, T. D. Harris, L. E. Brus, Nature 383, 802 (1996).

[6] V. I. Klimov, A. A. Mikhailovsky, D. W. McBranch, C. A. Leatherdale, M. G. Bawendi, Science 287, 1011 (2000).

[7] M. Kuno, D. P. Fromm, H. F. Hamann, A. Gallagher, D. J. Nesbittc, J. Chem. Phys. 115, 1028 (2001).

[8] A. Benda, M. Hof, M. Wahl, M. Patting, R. Erdmann, P. Kapusta, Review of Scientific Instruments 76, 033106 (2005).

[9] T. Dannhauser, M. O. Neil, K. Johansson, D. Whitten, G. J. McLendon, Phys. Chem. 90, 6074 (1986).

[10] G. Schlegel, J. Bohnenberger, I. Potapova, A. Mews, Phys. Rev. Lett. 88, 137401 (2002).

[11] Based on the TTTR measurements, we can obtain the distribution of fluorescence lifetimes with 200 ms integration time. In this case, Maximum likelihood Estimator fitting methods can be performed by using simple mono-exponential decay function of $I(t) = I_0 \exp(-\frac{t}{\tau})$.

Chapter 5: Fluorescence Enhancement by Phototreatment

I. Introduction

Colloidal CdSe QDs have attracted much attention due to excellent fluorescence (also called photoluminescence, PL) properties, including high quantum yields, size-dependent emission spectra, and good photostability.[1,2] The high surface to volume ratio makes fluorescence properties variable and sensitive to surface molecules,[3] local environments,[4-6] and light illumination.[7-9] Photoinduced fluorescence enhancement for *ensemble* colloidal CdSe QDs has been observed under various conditions, such as in aqueous and organic solutions,[7,8] in aggregated QD monolayers,[9] in a polymer thin film,[10] or even just under exposure to ambient light (i.e. unintentionally illuminating by room light)[11] and has been extended to the single-QD levels.[12] Furthermore, the PFE phenomenon has been utilized to fabricate multilayer optical data storage.[13] However, the mechanism of PFE is still under debate. The main proposed mechanism *from ensemble viewpoints* was attributed to surface-environmental effect, such as photo-induced surface passivation by water molecules,[9] photo-induced surface transformation,[14] and photo-induced oxidation.[15] On the other hand, from the viewpoint of single QD, the emission efficiency is mainly influenced by the fluorescence blinking behavior.[16] The dark state (off-times) is ascribed to the formation of charged QDs, which can considerably quench the fluorescence by efficient energy transfer (Auger nonradiative recombination) from exciton annihilation to the excess charges within the QD.[17,18] Previous works have demonstrated that photoinduced ionization in single colloidal QDs can occur upon illumination by means of electrostatic force microscopy.[19~22] Some of the single QDs can exhibit a positive charge upon illumination. Therefore, fluorescence should be quenched rather than enhanced upon light illumination by the formation of charged

QDs. This finding seems to be inconsistent with the ensemble PFE phenomenon based on single-QD fluorescence blinking mechanism. It also indicates that the photogeneration of charged carriers should play an important role in PFE phenomenon. Consequently, in order to unravel this issue, it is necessary to investigate the fluorescence properties down to single-QD levels.

II. Results and discussion

Figure 5.1 (a) shows the fluorescence spectra of ensemble colloidal CdSeTe/ZnS core/shell QDs on the glass coverslip at ambient environment with various illumination times. The fluorescence intensity increased monotonically and accompanied with a blue shift in the emission peak with the illumination time. Compared with the un-illuminated QDs, the enhanced factor is 2.6 for 20 min illumination. Based on the increased intensity and peak blue shift, the enhancement of fluorescence is initially assigned to the surface passivation of trap states by oxidation.[15] After 20 min, the fluorescence intensity was saturated and no significant change in line shape was found. After 6 hours in the dark, 85% of the enhanced fluorescence intensity was maintained. To eliminate the oxidation effect, we also performed the fluorescence measurements in vacuum under the same experimental conditions. Figure 5.1 (b) shows the fluorescence spectra of ensemble colloidal CdSeTe/ZnS core/shell QDs on the glass coverslip in vacuum with various illumination times. In general, the fluorescence intensity was decreased upon the evacuation of air.[6] Interestingly, the PFE behavior can be still obervsed, but with a smaller enhanced factor. No significant change in the peak position and line-shape were found. It indicates that the surface oxidation is not the only cause of the PFE phenomenon. There must be another effect to cause the PFE behavior. The heating effect was excluded because the fluorescence intensity should decrease with rising temperature.[14] Therefore, it is believed that the photoinduced charge carriers can play an important role in the PFE mechanism due to modifications of the single-QD fluorescence blinking behavior.

In order to unravel this PFE mechanism, the fluorescence variations at the single-QD levels were studied by monitoring the fluorescence blinking behavior with/without illumination. Figure 5.2 displays the representative fluorescence

intensity images of a 4×4 μm^2 (150 pixels by 150 pixels, integration time of 0.6 ms/pixels) (a) without and (b) with 20 min illumination. Some of the individual QDs with initially weak emission can be enhanced by illumination (marked by red circles, hereafter referred to as PFE QDs). On the other hand, some of the individual QDs with initially strong emission maintain their original fluorescence intensity with no considerable change (green rectangles). Moreover, the fluorescence was quenched for a portion of single QDs after illumination (yellow circles). This work mainly focuses on these PFE individual QDs. For single-QD experiments, to avoid dots to dots heterogeneity (size, shape, and local nano-environments) within the inhomogeneous samples, more than 30 PFE individual QDs were measured to determine their average behavior.

Figure 5.3 (a) reveals the typical fluorescence time trace with 100 ms bin time for a representative PFE colloidal CdSeTe/ZnS QD. The inset shows the fluorescence time trace for a un-illuminated QD for comparison. For un-illuminated QDs, the blinking behavior exhibits the simple two-states (on/off) transition with very fast transition rates (i.e. with relatively short on-times) and with average counts of ~18 per bin, as shown in Fig. 5.3 (b). According to theoretical simulation by Verberk,[23] this fluorescence blinking feature is attributed to exciton emission from the true neutral core/shell QDs. In contrast, the fluorescence time traces of PFE QDs revealed relatively long on-times and exhibited multi-level on-time states (i.e. with different fluorescence intensity for different on-times events for the same individual QDs, marked by green solid line). The fluorescence intensity for various on-time events for PFE individual QDs either are higher or lower than the fluorescence intensity for true neutral QD emission (un-illuminated QDs). Based on these experimental observations, this single-QD fluorescence is assigned to emission from neutral core/charged shell QD states.[23] It can also be reflected on the histograms of fluorescence intensity in Fig.

5.3 (c). Obviously, the histograms of fluorescence intensity for PFE QDs exhibited multi-level state distributions.

Based on both ensemble and single-QD fluorescence measurements, a possible model from *single-QD viewpoints* can be introduced to rationalize this PFE phenomenon. Previous report has demonstrated that photo-induced ionization in colloial CdSe QDs occurs after illumination with above the bandgap light. In this case, some of single QDs have a positive charge within the QDs.[19~22] This photo-induced ionization model is used to elucidate our experimental observations and to rationalize the contradiction between ensemble PFE phenomenon and single-QD blinking behavior. As illustrated in Fig. 5.4, upon illumination, photo-generated electrons can either passivate surface/interface trap states or can be ejected to outside trap states in the surrounding matrix, to prevent further ionization process by Coulomb blockage.[23] The former (photoinduced surface passivation) was evidenced by enhanced fluorescence for either ensemble or individual QD samples. The latter (suppression of further ionization) was proved by relatively long on-times in single-QD fluorescence time traces. On the other hand, counterpart holes either delocalized within the QD core to form the charged QD state (state 2, dark state) or trapped into the core/shell interface or on the shell surface (state 3, hereafter referred to as neutral core/charged shell states). According to the blinking models, charged QDs should not emit fluorescence photons due to energy transfer from exciton to excess charged carriers by efficient Auger recombination. Therefore, while the holes were delocalized within the QD core, it causes the quenched fluorescence (state 2, marked by yellow circle in fluorescence intensity images in Fig. 5.2). However, when the holes were localized on the surface far away from the core, the QDs can still emit fluorescence photons because of less wavefunction overlap between the delocalized exciton and the localized holes (the exciton wave-function decays exponentially into the shell, state 3).

Recently, Verberk *et al.* introduced charged shell/neutral core QD states to elucidate theoretically the relatively long on-time states in CdSe/ZnS core/shell QDs.[23] Actually, hole trap states were commonly observed in nanometer-size colloidal QDs because of their high surface to volume ratio. In previous studies, photogenerated holes which located on the surface or interface can migrate and cause the fluorescence intensity with multi-level states in fluorescence time traces.[24] In this case, the fluorescence intensity could range a broad distribution, which depends on the distance from the trapped hole to the core (different degrees of Auger recombination) and should be weaker than true neutral core states (state 1, no Auger recombination). However, the combination of both surface passivation and charged shell/neutral core QD states, single-QD fluorescence intensity in the fluorescence time traces may exceed the true neutral QD states (state 1). This finding is consistent with our experimental results. Therefore, we suggest that the origin of PFE phenomenon for colloidal CdSeTe/ZnS QDs is attributed to the overall contributions of both photoinduced surface passivation by photogenerated charged carriers and the formation of neutral core/charged shell QD states.

III. Conclusions

Photoinduced fluorescence enhancement in colloidal CdSeTe/ZnS core/shell QDs was studied by means of both ensemble and single-QD fluorescence measurements. Ensemble fluorescence intensity can be increased either in air or in vacuum, but with different enhanced factors. At the single-QD levels, fluorescence intensity was increased for some of individual QDs upon illumination. For these PFE individual QDs, relatively long on-times, high quantum yields within the on-times, and multi-levels on-states was found in fluorescence blinking time traces. Combination ensemble with single-QD fluorescence measurements, we proposed that the origin of PFE phenomenon is attributed to the both contributions of surface passivation by photo-induced charged carriers and formation of the neutral core/charged shell QD states.

(a)

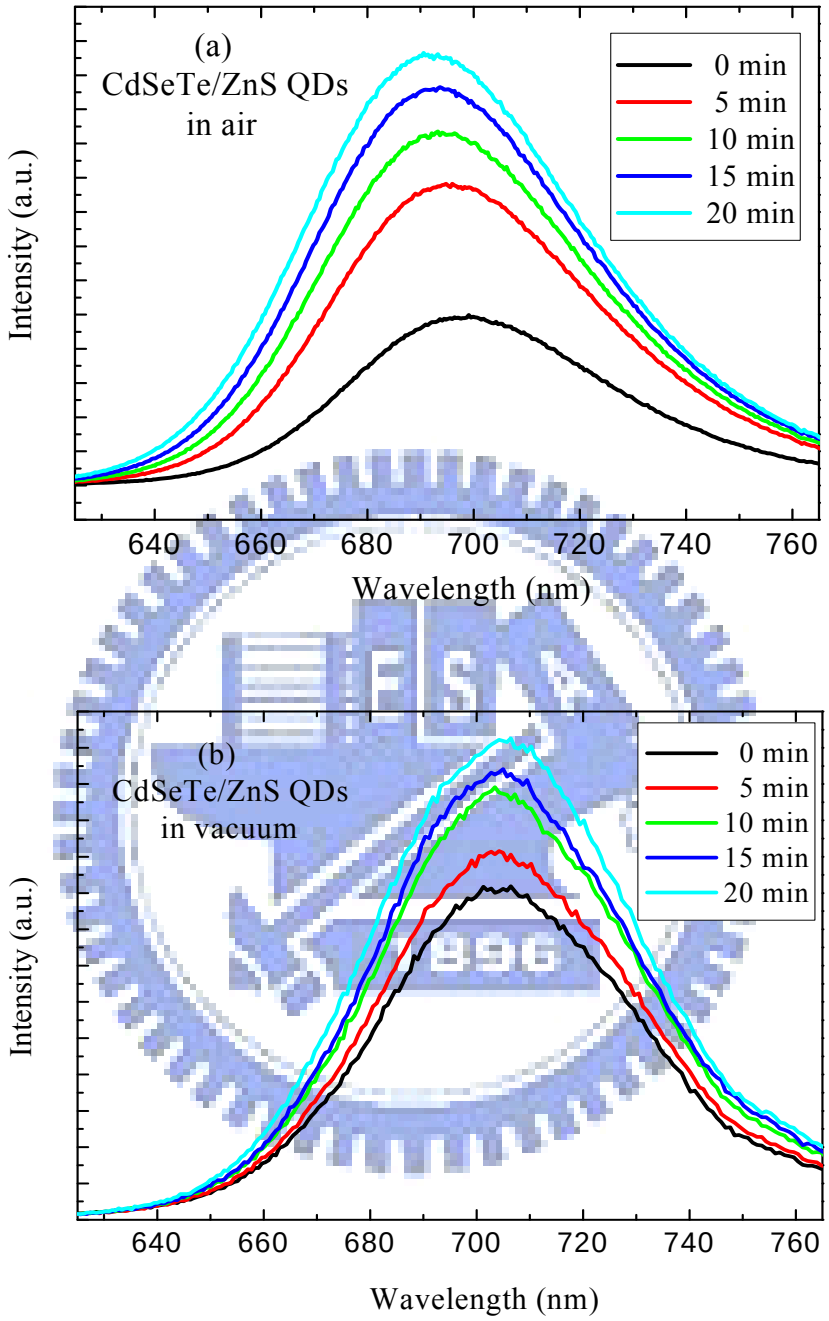

Figure 5.1: Fluorescence spectra of colloidal CdSeTe/ZnS QDs with various illumination times in air (a) and in vacuum (b).

(a)

(b)

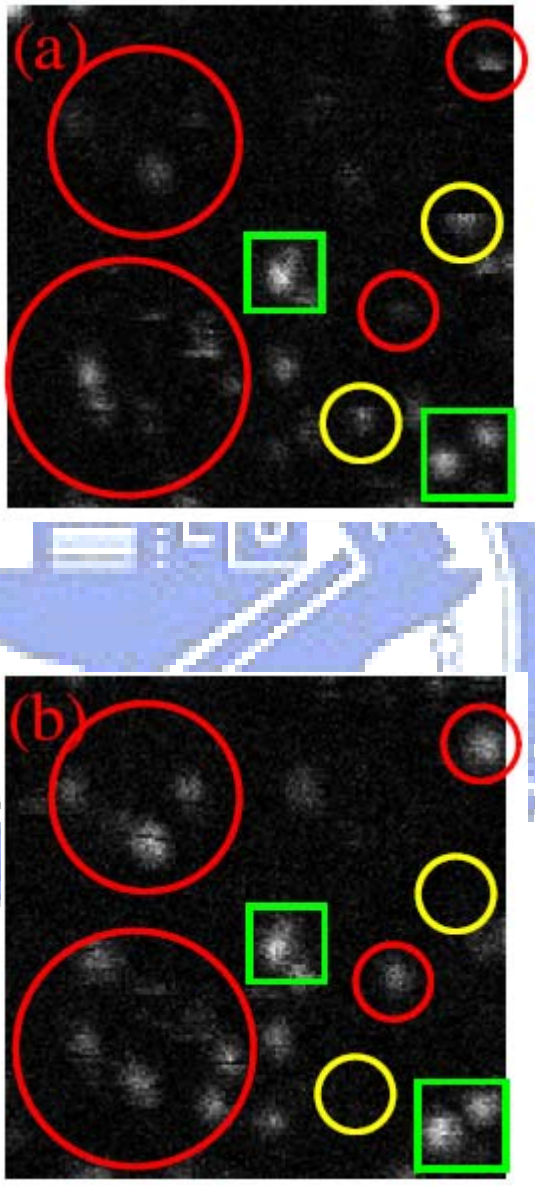

Figure 5.2: Fluorescence images without (a) and with 20 min illumination (b).

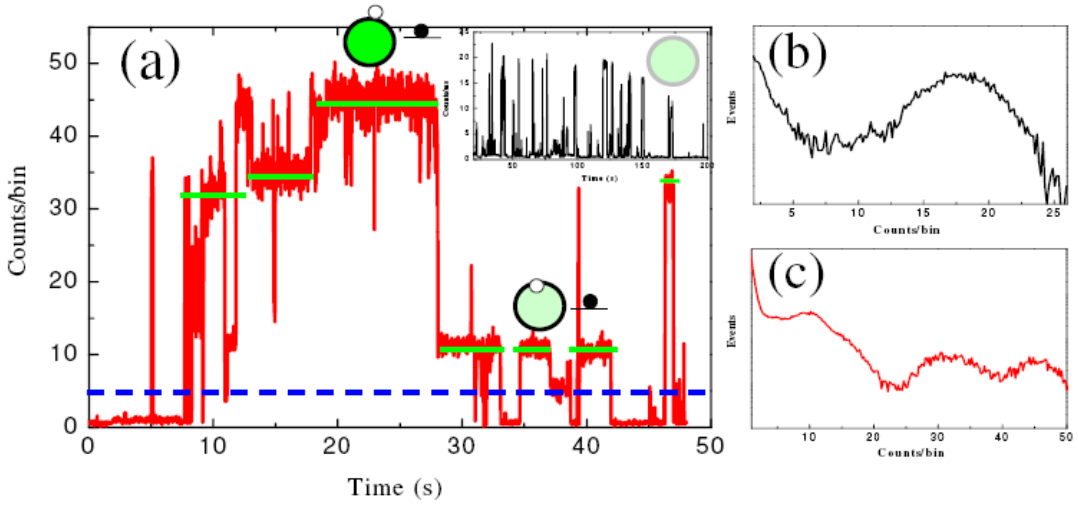

Figure 5.3: (a) Representative fluorescence time traces for single PFE QDs and unilluminated single QDs in the inset, (b) the distributions of events of fluorescence intensity for unilluminated QDs, (c) for PFE QDs.

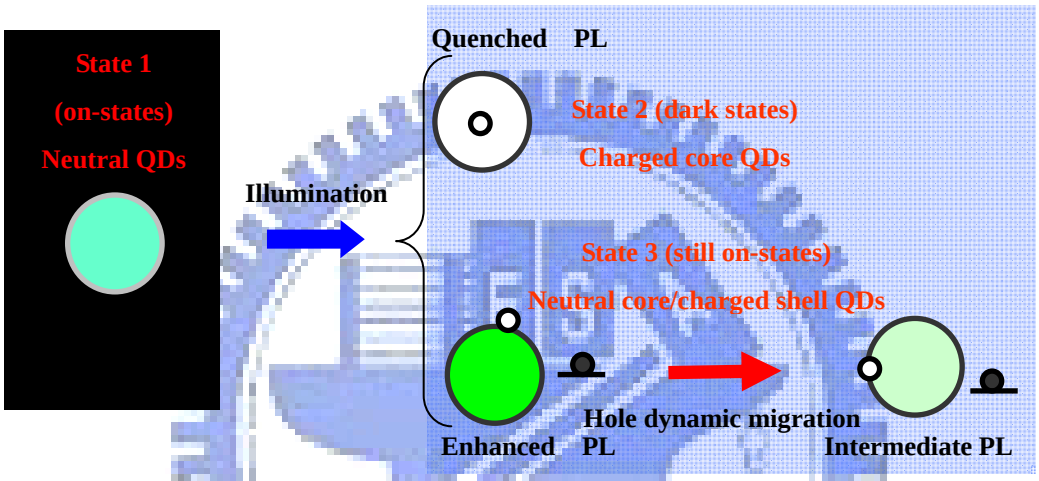

Figure 5.4: Schematic for PFE origin from single-QD viewpoints.

References

[1] M. J. Bruchez, M. Moronne, P. Gin, S. Weiss, and A. P. Alivisatos, Science 281, 2013 (1998).

[2] W. C. W. Chan, and S. M. Nie, Science 281, 2016 (1998).

[3] C. T. Yuan, W. C. Chou, Y. N. Chen, J. W. Chou, D. S. Chuu, C. A. Lin, J. K. Li, W. H. Chang, and J. L. Shen, J. Phys. Chem. C 111,15166 (2007).

[4] J. A. Kloepter, S. E. Bradforth, and J. L. Nadean, J. Phys. Chem. B 109, 9996 (2005).

[5] F. Koberling, A. Mews, and T. Basche, Adv. Mater. 13, 672 (2001).

[6] G. W. Shu, W. Z. Lee, I. J. Shu, J. L. Shen, C. A. Lin, W. H. Chang, R. C. Ruaan, and W. C. Chou, Nanotechnology, IEEE Transactions 4, 632 (2005).

[7] M. Jones, J. Nedeljkovic, R. J. Ellingson, A. J. Nozik, and G. J. Rumbles, J. Phys. Chem. B 107, 11346 (2003).

[8] M. Noseung, J. B. Yoon, and J. B. Allen, Nano Lett. 3, 747 (2003).

[9] S. R. Cordero, P. J. Carson, R. A. Estabrook, G. F. Strouse, and S. K. Buratto, J. Phys. Chem. B 104, 12137 (2000).

[10] A. Y. Nazzal, X. Wang, L. Qu, W. Yu, and Y. Wang, J. Phys. Chem. B 108, 5507 (2004).

[11] J. M. Tsay, S. Doose, F. Pinaud, and S. Weiss, J. Phys. Chem. B 109, 1669 (2005).

[12] Y. Wang, Z. Tang, M. A. Correa-Duarte, L. M. Liz-Marzan, and N. A. Kotov, J. Am. Chem. Soc. 125, 2830 (2003).

[13] J. W. M. Chon, P. Zijlstra, and M. Gu, Appl. Phys. Lett. 85, 5514 (2004)

[14] B. C. Hess, I. G. Okhrimenko, R. C. Davis, B. C. Stevens, Q. A. Schulzke, K. C. Wright, C. D. Bass, C. D. Evans, and S. L. Summers, Phys. Rev. Lett. 86, 3132 (1999).

[15] X. Wang, J. Zhang, A. Nazzal, and M. Xiao, Appl. Phys. Lett. 83, 162 (2003).

[16] M. Nirmal, B. O. Daboussi, M. G. Bawendi, J. J. Macklin, J. K. Trautman, T. D. Harris, and L. E. Brus, Nature 383, 802 (1996).

[17] A. L. Efros, and M. Rosen, Phys. Rev. Lett. 78, 1110 (1997).

[18] V. I. Klimov, A. A. Mikhailovsky, D. W. McBranch, C. A. Leatherdale, M. G. Bawendi, Science 287, 1011 (2000).

[19] T. D. Krauss and L. E. Brus, Phys. Rev. Lett., 83, 4840 (1999).

[20] T. D. Krauss, S. O. Brien, and L. Brus, J. Phys. Chem. B 105, 1725 (2001).

[21] O. Cherniavskaya, L. Chen, and L. Brus, J. Phys. Chem. B 108, 4946 (2004).

[22] O. Cherniavskaya, L. Chen, M. A. Islam, and L. Brus, Nano Lett. 3, 497 (2003).

[23] R. Verberk, A. M. Oijen, M. Orrit, Phys. Rev. B 66, 233202 (2002).

[24] K. Zhang, H. Chang, A. Fu, A. P. Alivisatos, and H Yang, Nano Lett. 6, 843 (2006)

Chapter 6: Electronic and vibrational states under high pressures

I. Introduction

Due to strong quantum confinements in all spatial directions, the emission colors can be tuned to cover whole visible range by changing the QD sizes. On the other hand, high pressure technique is another approach to vary the electronic levels of crystalline materials. Incorporation colloidal QDs under high pressure environment can provide valuable information to study the electronic and vibrational states of nanometer-sized materials. Previous reports have demonstrated that colloidal QDs exhibit distinct properties from bulk materials. For example, structural transformation of CdSe bulks from wurtzite to rock-salt occurred at the pressure of ~3 GPa.[1] In contrast to bulk CdSe, the structures of nanocrystals are stable at pressure above 5 GPa.[2~3] For both nanocrystals and bulk materials, the pressure-induced lattice constant variations are all linear relation which can be reflected in the pressure dependent optical measurements.[1~3] However, from the theoretical predictions,[4] the lattice constant variations under high pressures should follow quadratic relationship since the bulk modulus is a function of pressures. Surprisingly, this quadratic relationship was not observed explicitly in previous reports. One possible reason is that the limitation of structure phase transformation occurred before entering quadratic regime. To confirm this, it is necessary to delay the transformation pressure of samples. The elevation of transformation pressure can be achieved by the capping of ZnS.

The effect of ZnS capping on the delay of transformation pressure of CdSe nanocrystal can be illustrated by the thermodynamic arguments proposed by Tolbert and Alivisatos to explain the Wurzite (WZ) to rock-salt (RS) structure transformation of uncapped CdSe nanocrystals.[5] Surface energy, which depends on the inverse of

radius square, was accounted for the size dependent WZ to RS structure transition. The surface atoms, which have dangling bonds, are more energetic and unstable than those atoms inside the nanocrystal. As the external pressure was applied, the surface atoms play the role of nucleation sites for structure transformation. The nucleation sites decreases with the decreasing nanocrystal radius. As a result, the WZ to RS transformation pressure varies inversely with the square of CdSe nanocrystal radius and can be fitted by the thermodynamic model.[5] Although the capping of ZnS increases the strain energy due the lattice mismatched between ZnS and CdSe. More importantly, it greatly reduces the surface nucleation sites for the WZ to RS phase transition. In the case of SiO_2 coated Si nanocrystals, the semiconductor diamond structure to the metallic β-Sn structure transformation can be elevated from 11 GPa of bulk Si to 22 GPa.[6] In addition, the WZ to RS transformation pressure of ZnS is 17.4 GPa[7] and is much higher than that of bulk CdSe of 2.9 GPa.[8] Therefore, the delay of WZ to RS transformation pressure can be accomplished by the capping of ZnS. The crystal structure of capped CdSe nanocrystals is more stable than that of the uncapped CdSe nanocrystals of the same size. Furthermore, the capped CdSe/ZnS core/shell nanocrystals are optically more stable.[9]

To observe the pressure-induced quadratic variations of lattice constants, the colloidal CdSe QDs with ZnS thin capping layers were investigated under high pressures with de-ionized water as the pressure transmit medium. PL and Raman scattering measurements have been performed under various pressures up to ~7 GPa at room temperatures. Pressure-induced quadratic variations of lattice constants are observed explicitly from both PL and Raman scattering. The average pressure coefficients for PL and Raman measurements, as well as Gruneisen parameter are found to be 32 meV/GPa, 4.2 cm^{-1}/GPa and 0.11, respectively.

II. Results and discussion

Selected pressure dependent PL spectra are shown in Figure 6.1 and the corresponding high pressure values are marked in the figure. The main peaks are attributed to band edge emission of the QDs. The typical blue shift of PL peak positions can be observed with increasing pressures below ~7 GPa. However, as the pressure was applied above 7 GPa, the PL signal disappeared. It is ascribed to the semiconductor WZ to metallic RS transition occurs at 7 GPa. The pressure induced metallization was also observed in the resistance measurement of Zinc-blende (ZB) ZnSe at high pressure. As the semiconductor ZB ZnSe transforms to the RS structure at 13.5 GPa, its resistance drops 15 order of magnitude and it becomes metal.[10] In our previous paper, we found that when semiconductor ZB ZnSe transforms to metallic RS structure, the longitudinal optical (LO) phonon peak disappears suddenly.[14] Bulk CdSe also undergoes a phase transformation from semiconductor WZ to metallic RS structures at ~2.9 GPa.[8] In the case of core/shell CdSe/ZnS nanocrystals of 4 nm, the phase transformation occurs at 7 GPa. Above 7 GPa, nanocrystals become metal. The nanocrystal clusters transform from transparency (bright) to opaque (dark). As a result, the excitation of PL and lattice vibration by laser becomes impossible. No PL, 1LO, and 2LO phonon peaks can be detected. It is a reversible process, i.e., when the pressure was released, the PL and LO phonon signals recovered but exhibited hysteresis. The RS to WZ transformation during down-stroke process occurs at lower pressure than that of the up-stroke WZ to RS structure transformation. Tolbert and Alivisatos[5] found that Zinc-blende (ZB) is structurely isoenergetic to WZ phase. Both ZB and WZ phases were observed during the down-stroke process.

Figure 6.2 is a plot of the PL peak positions as a function of applied hydrostatic pressures. The pressure dependence quadratic relationship can be observed, that is, the slope decreases with increasing pressure. It implied that the pressure coefficient is not

a constant, but depends on the pressures. The equation $E(P) = E_0 + \alpha P + \beta P^2$ can be used to fit the overall experimental data. Here, α and β are average pressure coefficients. E_0=1.990 eV is the energy gap at ambient pressure and can be obtained by experiments. The fitting parameters for α 、β are 32 meV/GPa, and -1 meV/GPa^2, respectively. To compare with previous reports,[1~3] we divided the overall data into two parts, relative low and high pressure regimes. The threshold pressure is assigned to 3 GPa due to dramatic change of the slop. This threshold is just close to transition pressure of CdSe bulk. The linear function $E(P) = E_0 + \alpha P$ can be used to fit two regimes. The pressure coefficients α are 39 and 25 meV/GPa for low and high pressure regimes. The former is close to bulk value.[12] On the contrary, the latter resembles the value of nano-crystals.[2]

According to above findings, actually, there is a nonlinear factor that influences the relationship between PL peak positions and applied pressures. This effect can be explicitly observed in relative high pressure regime. We thus consider Murnaghan equation of state which describes the relation between applied pressures and lattice constants, $P = \frac{B_0}{B_0'}[(\frac{a_0}{a_0 + \Delta a})^{3B_0'} - 1]$, where B_0 and B_0' are the bulk modulus and its derivative with respect to P, a_0 is lattice constant under atmospheric pressure, Δa is the decrement of the lattice constants induced by the applied pressures. One can then obtain $P(\frac{\Delta a}{a_0}) = \frac{B_0}{B_0'}[(\frac{1}{1+\frac{\Delta a}{a_0}})^{3B_0'} - 1] = -3B_0(\frac{\Delta a}{a_0}) + 3B_0'[3B_0' - 1](\frac{\Delta a}{a})^2 + \text{high order}$ terms of $(\frac{\Delta a}{a})$. In general, for simplicity, the equation can be approximated to the form of $-3B_0(\frac{\Delta a}{a_0}) + 6B_0(\frac{\Delta a}{a_0})^2 +$ high order terms of $(\frac{\Delta a}{a})$ by choosing $B_0' \sim 1$. If the external applied pressure is high enough, the second order term cannot be neglected. Hence, the pressure-induced quadratic variations of lattice constants can be

reflected in the pressure dependent PL data of figure 6.2. From the viewpoint of volume change under applied pressures, bulk modulus is not a constant and increases with increasing pressures. It implies that colloidal QDs are getting harder to be compressed in relative high pressure regime. Therefore, the pressure coefficients are getting smaller.

For colloidal QDs under high pressures, the blue shift of the PL peak position is not only caused by the lattice contraction but also by the enhanced quantum confinement. For quantum confinement effect, the changes in electronic energy under applied pressure are given by $\Delta E = \frac{\hbar^2 \pi^2}{2\mu R^2}(\frac{1}{f} - 1)$,[13] where f is the volume compressive ratio due to pressures, μ is the reduced mass of electron and hole, and R is the radius of the QDs. By employing the typical parameters of CdSe QDs with 4 nm in radius and set f to be about 0.8, the change of the electron energy induced by the increasing of quantum confinement due to the applied pressure up to the phase transformation is still much small. This implies the blue shift of the PL peak position caused by the quantum confinement effect can be neglected.

Raman scattering measurement is a very sensitive and powerful tool to probe the lattice property of crystalline structures. To further study the pressure-induced lattice constant quadratic behavior, Raman spectra were also recorded at the same time. Figure 6.3 shows the Raman spectrum of colloidal CdSe/ZnS QDs under the pressure of 1.43 GPa at room temperatures. From left to right, three peaks can be observed, and are assigned as LO phonon of CdSe core, LO phonon of ZnS shell, and 2-LO phonon of CdSe, respectively. Figure 6.4 shows pressure dependent Raman spectra of colloidal CdSe/ZnS QDs under various high pressures. With the increasing of pressure, all phonon peaks shift to higher frequency up to 7 GPa. Above this pressure, these CdSe related Raman peaks disappear abruptly. However, the LO phonon of ZnS cap is

still observable above 7 GPa because the WZ to RS transformation pressure of ZnS is 17.4 GPa. Combining PL with Raman scattering, it is appropriate to conclude that the structures transformation occurs at this pressure. Figure 6.5 (a), (b) show the peak positions of Raman shift for the LO and 2 LO phonons of CdSe QDs as a function of applied pressures. Both curves are all in quadratic behavior. The solid line is a quadratic fit by equation of $\omega(P) = \omega_0 + \alpha P + \beta P^2$ to overall experimental data. The average pressure coefficient for Raman shift is 4.23 cm^{-1}/GPa, which is consistent with previous results of bare CdSe colloidal QDs.[3] This is a clear evidence for hydrostatic pressures applied to the colloidal QD core even over-coated with a ZnS thin layer. We can also observe that there are two pressure regimes with different slope divided at the pressure of 3 GPa. From the pressure dependent Raman spectra, the Gruneisen parameter can be derived by the equations of $\gamma = \frac{B_0}{\omega_0}\frac{d\omega}{dP}$, where B_0 is the bulk modulus and equal to 53 GPa for CdSe bulk.16 One then obtains γ=0.11, and the LO phonon frequency at ambient pressure is 216 cm^{-1}, which is larger than the bulk value of 213 cm^{-1}. The increased value is due to additional compressive stress resulted from the over-coated ZnS. Previous work has reported that QDs over-coated with ZnS are able to increase the Raman shift with a value of $2\,cm^{-1}$.[15]

III. Conclusions

We have studied the electronic and vibrational states of colloidal core/shell CdSe/ZnS QDs at room temperatures with high pressure optical measurements. Pressure-induced quadratic lattice variations can be observed explicitly from both the PL and Raman spectra up to ~7 GPa. This quadratic relationship is consistent with the theoretical prediction. The average pressure coefficients for PL and Raman measurements, as well as Gruneisen parameter are obtained to be 32 meV/GPa , 4.2 cm^{-1}/GPa and 0.11, respectively.

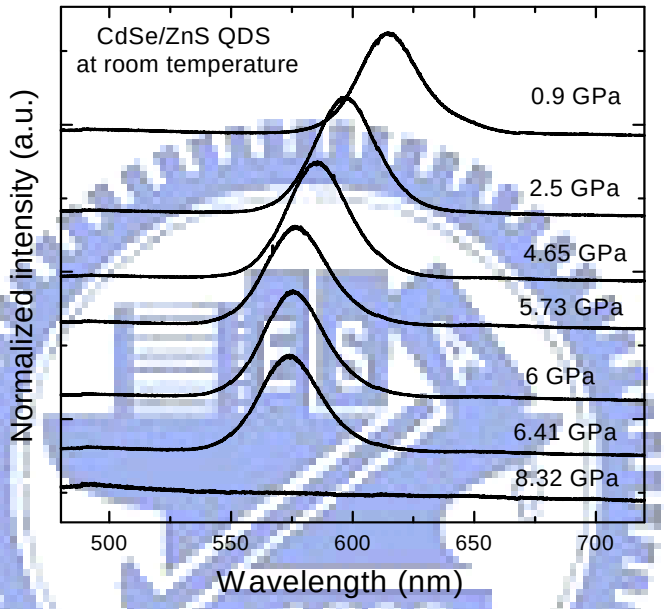

Figure 6.1: Pressure dependent PL spectra of colloidal CdSe/ZnS QDs at room temperature.

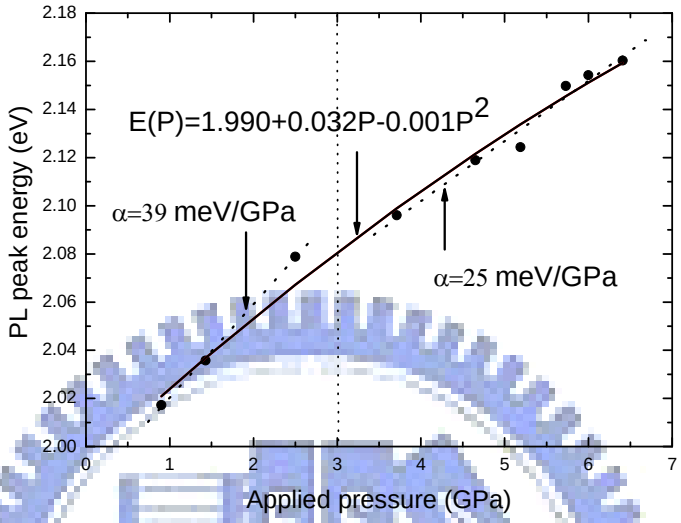

Figure 6.2: PL peak energy as a function of applied pressures.

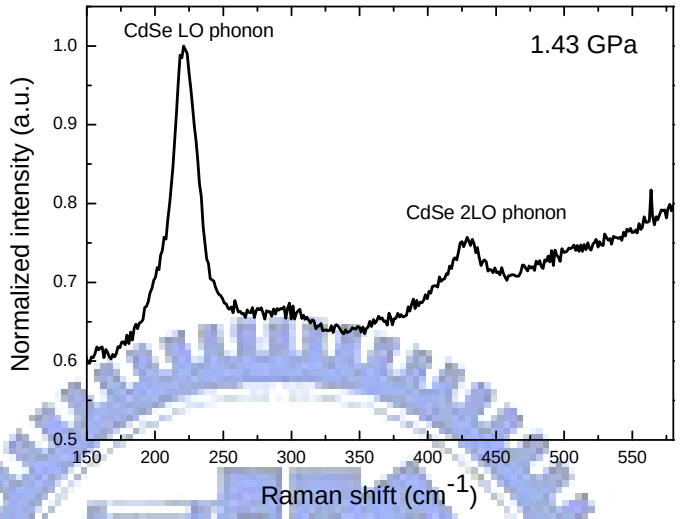

Figure 6.3: Raman spectrum of colloidal CdSe/ZnS QDs at 1.43 GPa at room temperature.

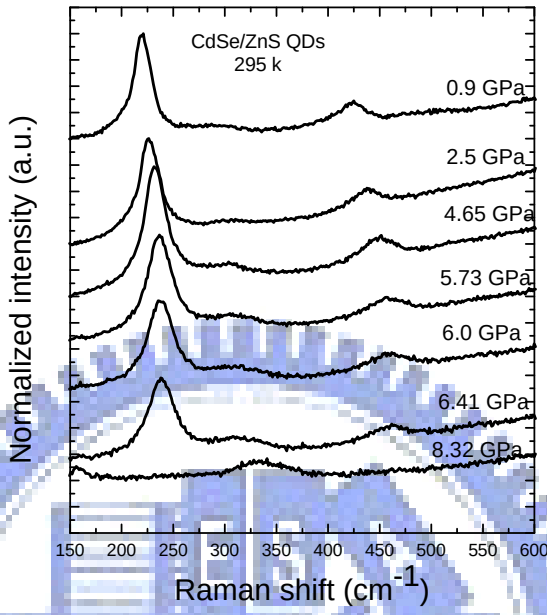

Figure 6.4: Pressure dependent Raman spectra of colloidal CdSe/ZnS QDs at room temperature.

(a)

(b)

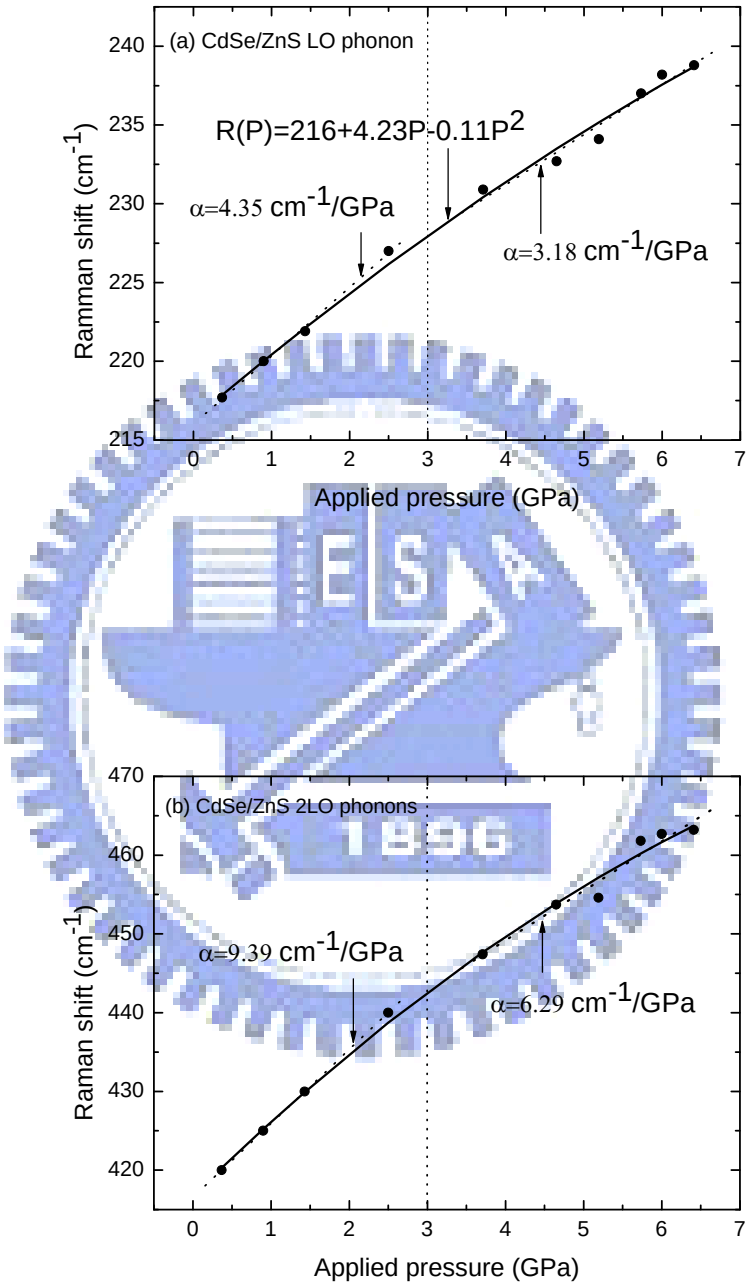

Figure 6.5: Raman peak shifts of (a) LO and (b) 2 LO phonon as a function of applied pressure.

References

[1] W. Shan, W. Walukiewicz, J. W. Ager, K. M. Yu, and J. Wu, Appl. Phys. Lett. **84**, 67 (2003).

[2] J. Li, G. H. Li, J. B. Xia, J. B. Zhang, Y. Lin and X. R. Xiao, J. Phys. Condens. Matter **13**, 2033 (2001).

[3] A. P. Alivisatos, T. D. Harris, L. E. Brus, and A. Jayaraman, J. Chem. Phys. **89**, 5979 (1988).

[4] S. H. Wei and A. Zunger, Phys. Rev. B **60**, 5404 (1999).

[5] S. H. Tolbert and A. P. Alivisatos, J. Chem. Phys. **102**, 4642 (1995).

[6] S. H. Tolbert, A. B. Herhold, C. S. Johnson, and A. P. Alivisatos, Phys. Rev. Lett. **76**, 4384 (1996).

[7] W. H. Gust, J. Appl. Phys. 53, 4843 (1982).

[8] J. R. Mei and V. Lemos, Solid State Commun. 52, 785 (1984).

[9] D. V. Talapin, A. L. Rogach, A. Kornowski, M. Haase, H. Weller, Nano Letter. 1, 207 (2001).

[10] G. Itkin, G. R. Hearne, E. Sterer, M. P. Pasternak, and W. Potzel, Phys. Rev. B 51, 3195 (1995).

[11] C. M. Lin, D. S. Chuu, T. J. Yang, W. C. Chou, J. Xu, and E. Huang, Phys. Rev. B 55, 13641 (1997).

[12] A. L. Edwards and H. G. Drickamer, Phys. Rev. **122**, 1149 (1961).

[13] Y. Kayanuma and H. Momiji, Phys. Rev. B **41**,10261 (1990).

[14] S. H. Wei, A. Zunger, Phys. Rev. B **60**, 5404 (1999).

[15] R. W. Meulenberg, Phys. Rev. B **70**, 235311 (2004).

Chapter 7: Fluorescent Properties of Single Gold Nano-clusters

I. Introduction

Noble-metal nanoparticles (NPs) with sizes ranging from 10 nm to 100 nm have been investigated extensively due to their strong optical absorption and scattering in the visible range (~520 nm for gold NPs and ~400 nm for silver NPs) caused by the collective oscillation of free electrons within the NPs (called localized surface plasmon resonance, LSPR).[1] This coherent electron motion generates the localized surface plasmon absorption and decays nonradiatively by electron-electron collisions on the timescale of ~femtoseconds. Many biological applications, such as markers and sensors,[2,3] have been achieved based on the single-particle LSPR. The resonant frequency depends on the size and shape of the NPs and the dielectric constant of the surrounding medium. To probe the optical scattering light from NPs, the total internal reflection microscopy[4] was generally used. The advantages of using gold NP scattering light for applications in biological markers are their biocompatibility, non-toxicity, good photostability (no photobleaching) and non-blinking. However, the intensity of scattering cross-section varies as sixth power of the NP size.[4] It implies that the LSPR intensity decreases considerably and becomes useless when the NP size reduces down to ~10 nm. Unfortunately, most biological molecules of interest have the sizes of ~nanometers or less. In order to have strong detection signal for the small metal NPs conjugated to biological molecules, other efficient emission mechanisms are to be explored urgently.

Recently, absorption cross-section and fluorescence were found to vary only as third power of size for metal NPs with relatively smaller sizes.[5] Due to their non-toxicity, smaller metal NPs or nanoclusters (NCs) gain overwhelming attention to CdSe colloidal semiconductor quantum dots (QDs) for future applications in

biological markers even though CdSe QDs have excellent fluorescence properties, such as size-dependent emission spectra and good photostability.[6] Consequently, fluorescent gold NCs are the promising candidates for future applications in biological markers because they are greener as well as fluorescent.

In fact, fluorescence from metal materials have been observed for more than 30 years.[7] However, it did not attract much attention due to very low quantum yields (QYs) of ~10^{-10}. This low QY is likely attributed to nonradiative relaxation processes due to very fast electron-electron scattering. Recently, fluorescence with relatively high QYs (10^{-4}~10^{-5}) was observed in small metal NPs (< 100 nm)[8] and metal nanoclusters (NCs, < 1 nm).[9] For gold NPs, the origin of fluorescence is tentatively assigned to radiative emission of excited LSPR due to their similar characteristics.[8] Alternatively, for fluorescent gold NC consisting of only a few atoms, LSPR behavior disappears due to the fact that a small number of free electrons can not generate collective oscillation. Therefore, the fluorescence from gold NCs is likely due to electronic state transition and still under investigation.

In this work, fluorescence properties of gold NCs were investigated, in particular, down to single-NC levels. Photoinduced fluorescence enhancement was found for ensemble gold NCs in solution, but NCs exhibited photobleaching phenomenon at ambient environments. At the single-NC levels, fluorescence blinking was observed and the distribution of on/off-times also follows the power-law similar to colloidal CdSe QDs. Moreover, the fluorescence decay profiles for single NCs show mono-exponential decay behavior with lifetime of ~7 ns.

II. Results and discussion

Figure 7.1 (a), (b) shows the absorption and fluorescence spectra of ensemble gold NCs in solution. Obviously, no LSPR feature can be found in the visible range, instead broad absorption band was observed in the ultraviolet range. It implies that fluorescence is not attributed to radiative emission by excitation of LSPR. The origin of this fluorescence is likely due to the transition of molecule-like electronic levels.[7] Fluorescence lineshape is not symmetric and has a broad linewidth. This broad linewidth originates from the distribution of sizes within the ensemble-heterogeneous gold NCs.[9] Moreover, stoke-shift of more than 200 nm was found and significantly larger than conventional fluorescent molecules.

In order to estimate the photostability of gold NCs, fluorescence intensity as a function of time was measured based on TTTR acquisition mode.[10] Figure 7.2 shows the variations of fluorescence intensity with illumination time for ensemble gold NCs in solution (a) and at ambient environment (b, evaporation of solvent). Ensemble gold NCs in solution are very photo-stable and photo-induced fluorescence enhancement was observed for long-time illumination. This photo-enhancement behavior is generally assigned to photo-induced surface passivation and has been widely found for colloidal CdSe QDs[11~13] and silver nanoparticles.[14] However, when the solvent was evaporated, fluorescence intensity dropped rapidly with illumination time. This photo-beaching phenomenon is similar to conventional organic molecules.

To get more insight into fluorescence properties, single-molecule detection (SMD) technique was used to study single NCs within the heterogeneous-ensemble samples. Based on this SMD technique, single-NC behavior can be highlighted and inter-NC interaction was diminished thus, intrinsic properties can be obtained. Figure 7.3 displays the fluorescence intensity images of $4\times4\mu m^2$ for gold NCs. Diffraction-limited spots with streaky pattern can be seen due to fluorescence

blinking and some of spots exhibit incomplete shape because of fast photobleaching during scanning processes. Figure 7.4 (a) shows the typical fluorescence time traces of a single NC for total measured time duration. At the beginning, reversible on/off blinking behavior can be seen clearly as shown in Fig. 7.4 (b) and then irreversible photo-bleaching occurred for long-time illumination. However, not all NCs can record blinking statistics, some of them suffered from too fast photo-bleaching to record statistical data. To get quantitative information about this blinking statistics, we adopted the conventional method for colloidal CdSe QDs to select a proper threshold intensity to separate on/off-times. Thus, on/off-time histograms can be constructed. Figure 7.5 (a)/(b) shows the histograms of on/off-time length for compiling more than 20 individual NCs. This relation can also be fitted by a simple power-law of $P(t) = At^{-\alpha}$ similar to CdSe QDs with on and off exponent of 2 and 1.8, respectively. The blinking mechanisms for single molecules and colloidal CdSe QDs have been widely investigated.[15~19] For some single molecules, their blinking on/off-times exhibit pure single-exponential distribution and can be explained to simple three level models (ground states, first excited states, triplet states). For colloidal CdSe QDs, the blinking statistics also follow the power-law and were tentatively elucidated by charge ionization/neutralization processes.[15~19] In current status, the blinking mechanism for single gold NCs is to be explored.

On the other hand, based on TTTR measurements, we also recorded fluorescence decay profiles of ensemble-aggregated gold NCs (a) and single non-interacting NCs (b). For ensemble-aggregated NCs, the bi-exponential decay function fits the experimental results with shorter and longer lifetime of 0.5 ns and 6 ns, respectively. In contrast to ensemble NCs, fluorescence decay curves of single NCs exhibit mono-exponential profiles with a lifetime of ~7 ns. Comparing ensemble and single-NC experimental results, we suggest that a single-NC exhibit

mono-exponential decay behavior and fast decay observed in ensemble measurements was likely due to energy transfer from small NCs to larger NCs (dipole-dipole interaction). The interaction is in nanometer range, thus can be observed for aggregated NCs and disappears for individual isolated NCs.

III. Conclusions

Fluorescence properties of gold NCs were investigated, in particular, down to single-NC level. Photo-induced fluorescence enhancement was found for ensemble gold NCs in solution, but ensemble gold NCs at ambient environment exhibits photo-bleaching phenomenon. At the single-NC levels, fluorescence blinking was observed and the distribution of on/off-times also follows the power-law similar to CdSe QDs. Moreover, the fluorescence decay profiles for single NCs show mono-exponential decay behavior with lifetime of ~7 ns.

(a)

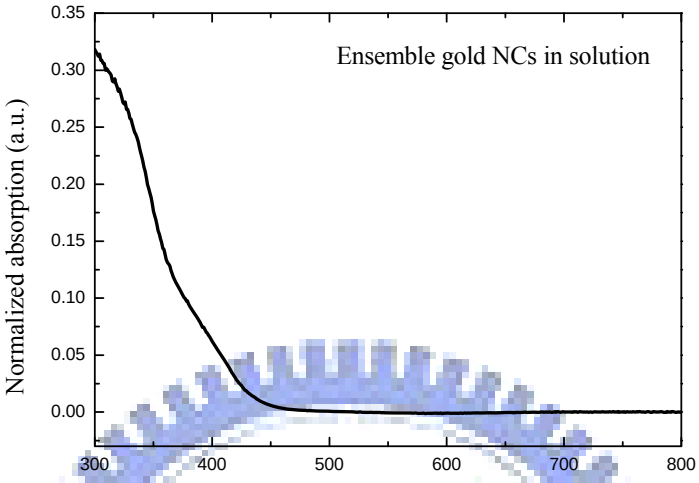

(b)

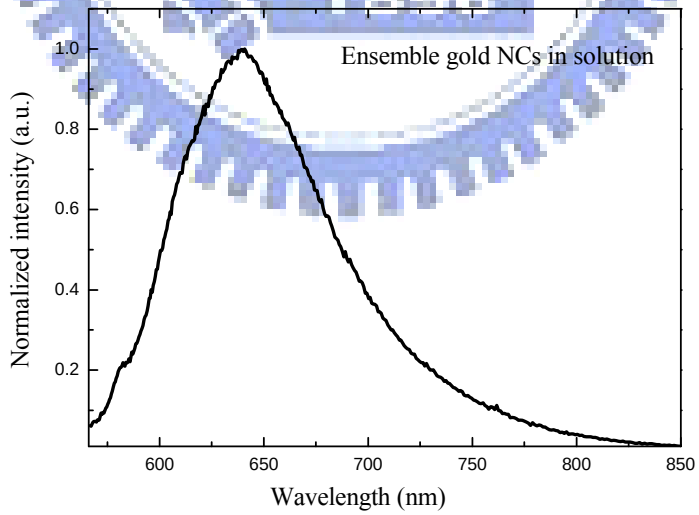

Figure 7.1: Absorption (a) and emission spectra (b) for ensemble gold NCs in solution.

(a)

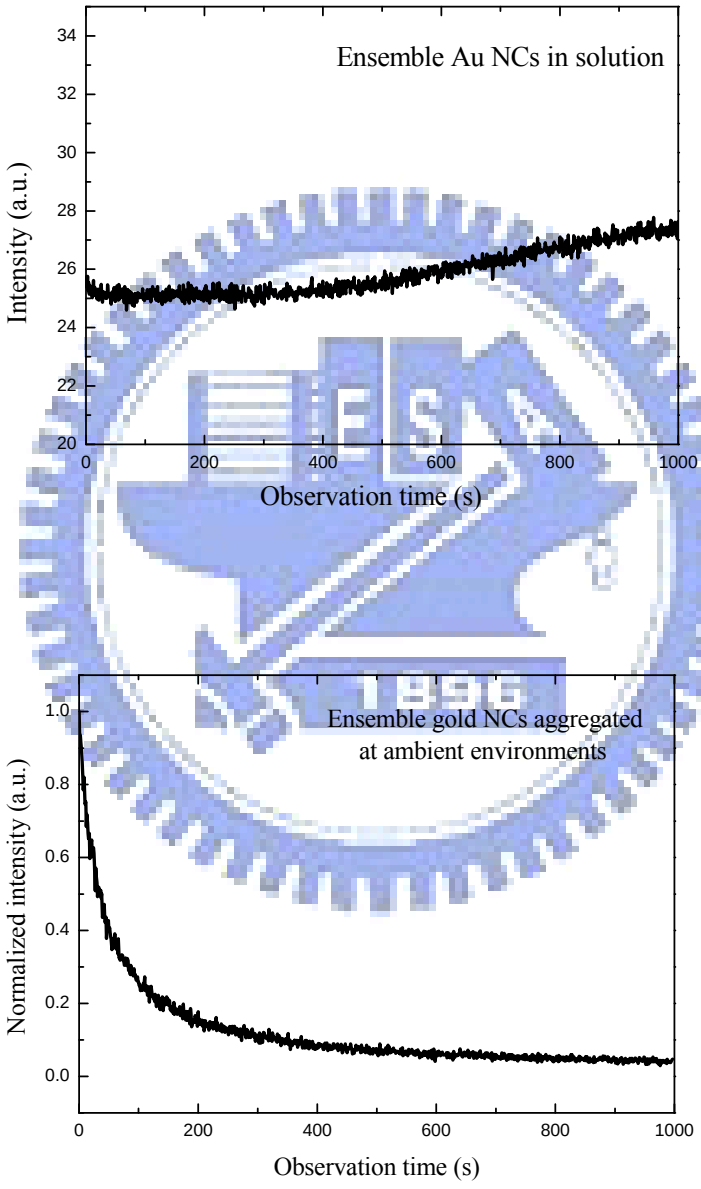

(b)

Figure 7.2: Fluorescence intensity variations with time in solution (a) and at ambient environment (b).

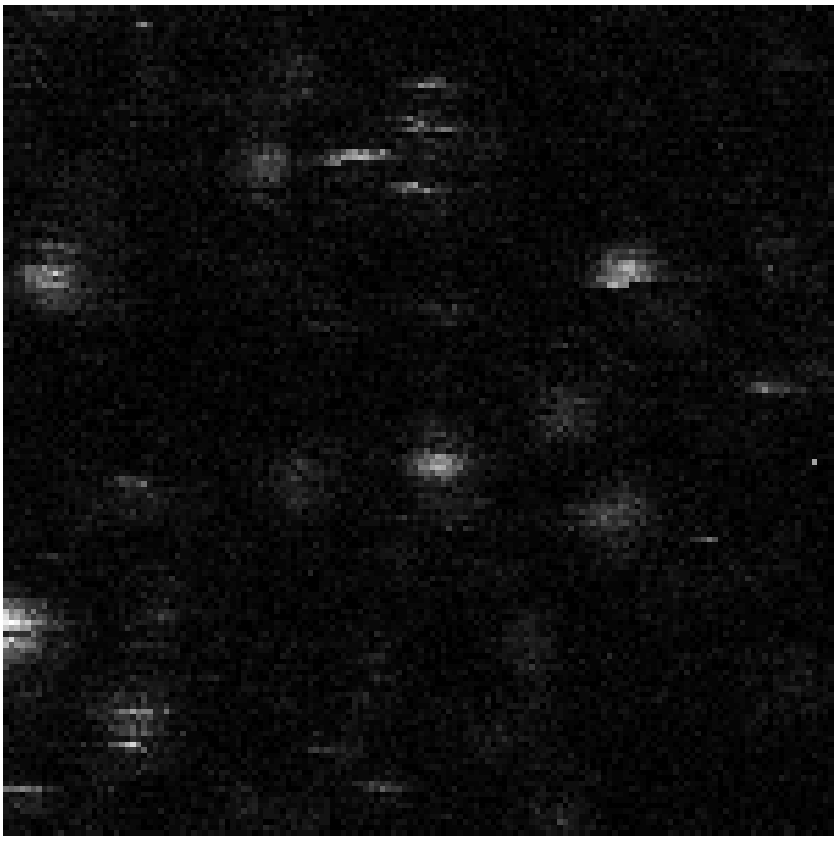

Figure 7.3: Fluorescence intensity images with $4 \times 4 \mu m^2$ for single NCs.

(a)

(b)

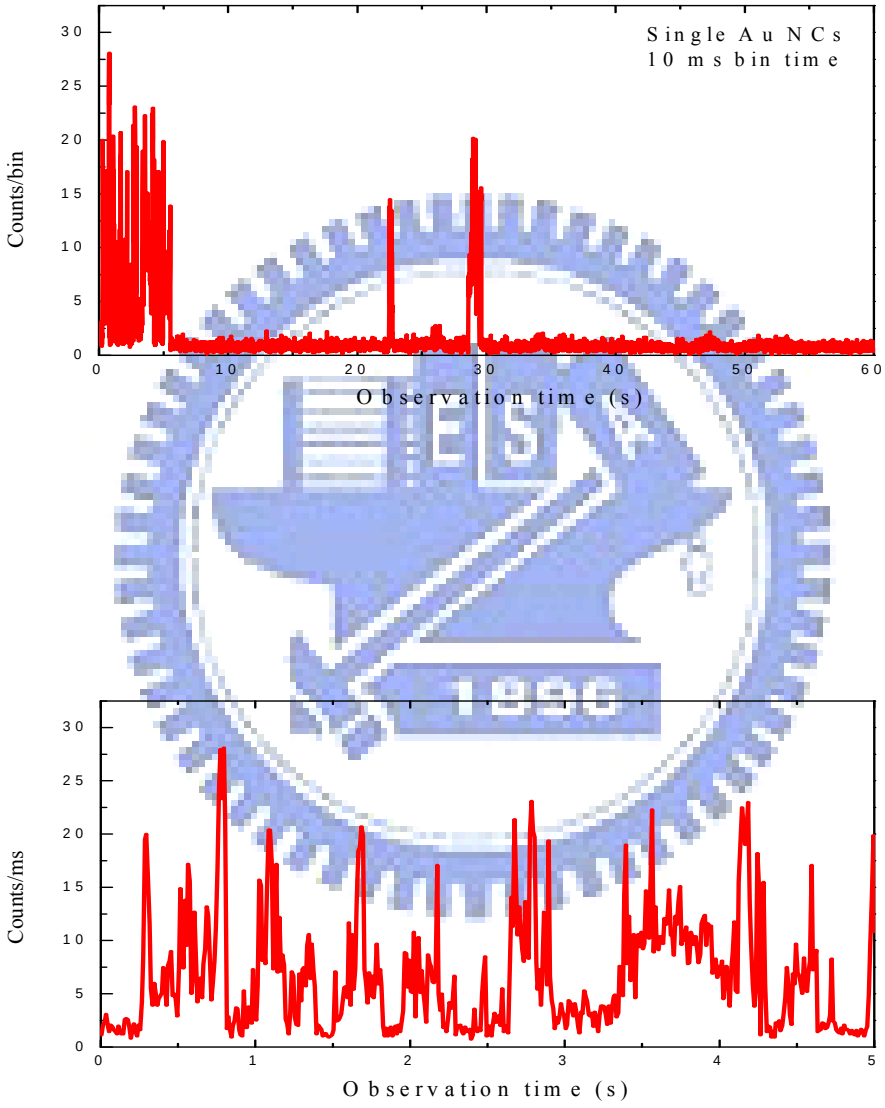

Figure 7.4: Fluorescence time traces for single NCs for total measured time (a) and initial 5 s time window (b).

(a)

(b)

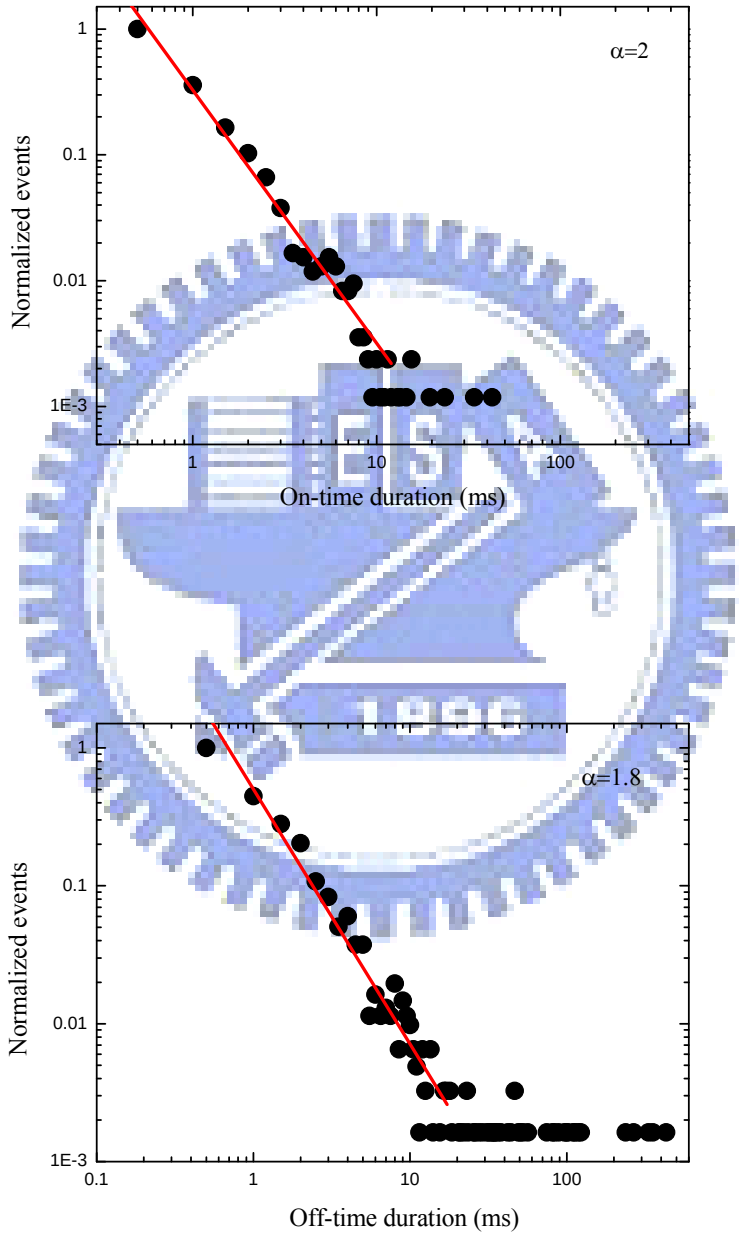

Figure 7.5: A plot of histograms of on-time duration (a) and off-time duration (b).

(a)

(b)

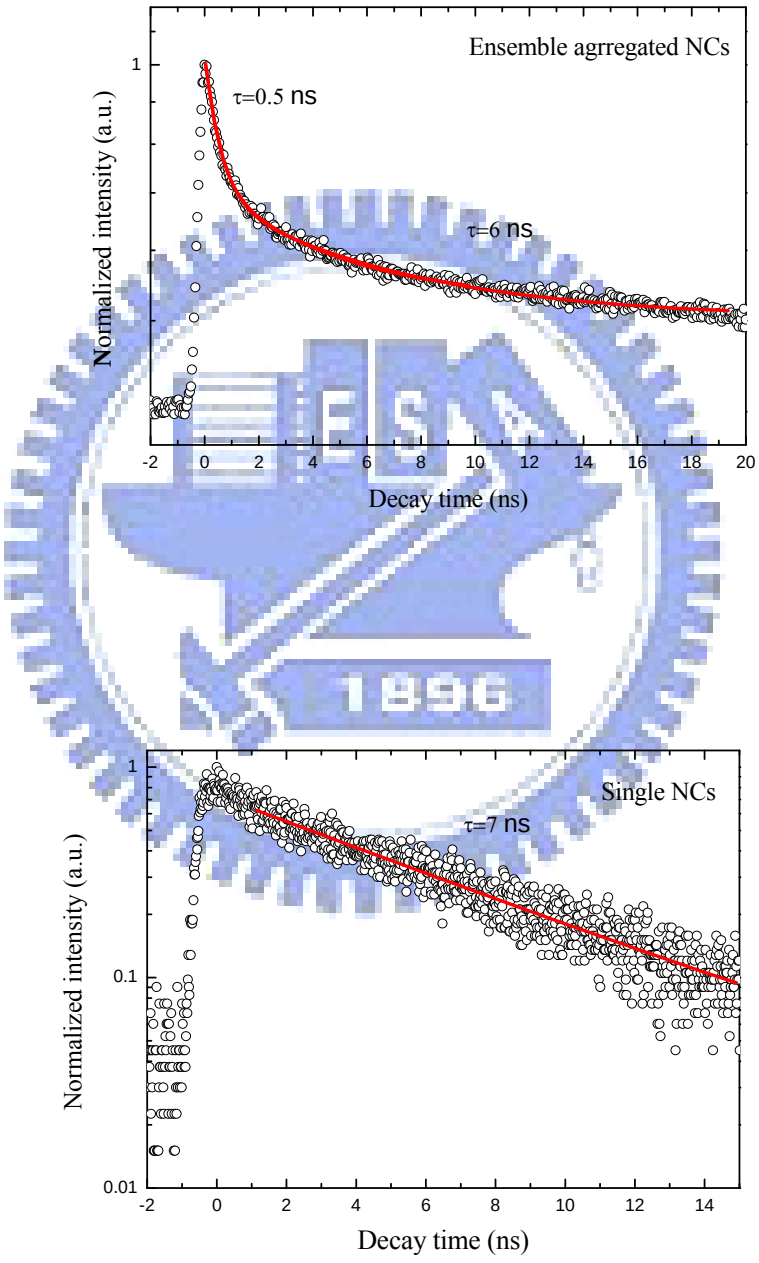

Figure 7.6: Fluorescence decay profiles of ensemble aggregated NCs (a) and single NCs (b).

References

[1] E. Fort and S. Gresillon, J. Phys. D 41, 013001 (2008).

[2] S. Schultz, D. R. Smith, J. J. Mork, D. A. and Schultz, Proc. Natl. Acad. Sci. 97, 996 (2000).

[3] A. D. McFarland and R. P. VanDuyne, Nano Lett. 3, 1057 (2003).

[4] M. A. VanDijk, M. Lippitz, and M. Orrit, Acc. Chem. Res. 38, 594 (2005).

[5] L. A. Peyser, A. E. Vinson, A. P. Bartko, and R. M. Dickson, Science 291, 103 (2001).

[6] M. Bruchez Jr, M. Moronne, P. Gin, S. Weiss, A. P. Alivisatos, Science 281, 2013 (1998).

[7] A. Mooradian, Phys. Rev. Lett. 22, 185 (1969).

[8] E. Dulkeith, T. Niedereichholz, T. A. Klar, and J. Feldmann, Phys. Rev. B 70, 205424 (2004).

[9] J. Zheng, C. Zhang, and R. M. Dickson, Phys. Rev. Lett. 93, 077402 (2004).

[10] A. Benda and M. Hof, Rev. Sci. Instrum. 76, 033106 (2005).

[11] M. Noseung, J. B. Yoon, and J. B. Allen, Nano Lett. 3, 747 (2003).

[12] S. R. Cordero, P. J. Carson, R. A. Estabrook, G. F. Strouse, and S. K. Buratto, J. Phys. Chem. B 104, 12137 (2000).

[13] C. T. Yuan, W. C. Chou, Y. N. Chen, C. A. Lin, and W. H. Chang, Appl. Phys. Lett. 92, 183108 (2008).

[14] C. D. Geddes, A. Parfenov, I. Gryczynski, and J. R. Lakowicz, J. Phys. Chem. B 107, 9989 (2003).

[15] M. Kuno, D. P. Fromm, H. F. Hamann, A. Gallagher, and D. J. Nesbitt, J. Chem. Phys. 115, 1028 (2001).

[16] M. Kuno, D. P. Fromm, H. F. Hamann, A. Gallagher, and D. J. Nesbitt, J. Chem. Phys. 112, 3117 (2000).

[17] M. Kuno, D. P. Fromm, S. T. Johnson, A. Gallagher, and D. J. Nesbitt, Phys. Rev. B 67, 125304 (2003).

[18] J. Tang and R. A. Marcus, Phys. Rev. Lett. 95, 107401 (2005).

[19] J. Tang and R. A. Marcus, J. Chem. Phys. 123, 054704 (2005).

Chapter 8: Conclusions

In this thesis, we have given an overview of advantages and disadvantages for nanometer-sized materials, including colloidal semiconductor QDs, metal NPs, and metal NCs for applications in biological labels and sensors. The common features for these nanometer-sized materials are the size and surface effects. In addition to intrinsic properties, surface plays an important role in determination of fluorescence properties, including QYs, spectra, and photostability. Single-molecule detection technique is a powerful tool to investigate these nanomaterials. Combining SMD and TTTR acquisition modes, we can obtain wealthy information such as fluorescence time traces, fluorescence lifetime, fluorescence intensity and lifetime images. Therefore, we utilized this technique to investigate the fluorescence properties for single QDs and metal NCs.

In order to enhance fluorescence intensity of single CdSe/ZnS QDs, HDA molecules have been used to modify the QDs surfaces. In this case, ensemble fluorescence intensity was increased and single-QD blinking behavior can be dramatically modified. The on/off time ratios and the total number of emitted photons within the on-time duration can be enhanced up to 2.8 and 13-fold, respectively. Consequently, the blinking rate can be suppressed down to 18%. The fluorescence decay curve exhibits more close to single exponential decay profile and has longer measured lifetime. These results suggested that HDA ligands can provide the higher degree of surface passivation.

Phototreatment is another way to enhance fluorescence intensity for ensemble QDs. Here, core/shell CdSeTe/ZnS QDs were illuminated by a 480 nm light and ensemble QYs can be enhanced either at ambient environment or in vacuum. At the single-QD levels, fluorescence intensity was increased for some of individual QDs upon

illumination. For these PFE individual QDs, relatively long on-times, high quantum yields within the on-times, and multi-levels on-states was found in fluorescence blinking time traces. Combination ensemble with single-QD fluorescence measurements, we proposed that the origin of PFE phenomenon is attributed to the both contributions of surface passivation by photo-induced charged carriers and formation of the neutral core/charged shell QD states.

Furthermore, we have also studied the electronic and vibrational states of colloidal core/shell CdSe/ZnS QDs at room temperatures with high pressure optical measurements. Pressure-induced quadratic lattice variations can be observed explicitly from both the PL and Raman spectra up to ~7 GPa. This quadratic relationship is consistent with the theoretical prediction. The average pressure coefficients for PL and Raman measurements, as well as Gruneisen parameter are obtained to be 32 meV/GPa , 4.2 cm^{-1}/GPa and 0.11, respectively.

Finally, fluorescent gold NCs were investigated, in particular, down to single-NC levels. Photoinduced fluorescence enhancement was found for ensemble gold NCs in solution, but exhibited photobleaching phenomenon at ambient environments. At the single-NC levels, fluorescence blinking was observed and the distribution of on/off-times also follows the power-law similar to CdSe QDs. Moreover, the fluorescence decay profiles for single NCs show monoexponential decay behavior with lifetime of ~7 ns.

Publication lists

1. Photoinduced fluorescence enhancement in colloidal CdSeTe/ZnS core/shell QDs, **C. T. Yuan**, W. C. Chou, Y. N. Chen, C. A. Lin, and W. H. Chang, Appl. Phys. Lett. 92, 183108 (2008). (also selected for the May 19, 2008 issue of Virtual Journal of Nanoscale Science & Technology).
2. Temperature dependence of excitonic emission in cubic thin film, C. H. Chia, **C. T. Yuan**, J. T. Ku, S. L. Yang, W. C. Chou, J. Y. Juang, S. Y. Hsieh, K. C. Chiu, J. S. Hsu, and S. Y. Jeng, Journal of Luminescence, 128, 123 (2008).
3. Study of fluorescence enhancement of colloidal CdSe/ZnS QDs bound to hexadecylamine by single-molecule measurements, **C. T. Yuan**, W. C. Chou, Y. N. Chen, J. W. Chou, D. S. Chuu, C. A. Lin, J. K. Lin, W. H. Chang, and J. L. Shen, J. Phys. Chem. C, 111, 15166 (2007).
4. Studies on the electronic and vibrational states of colloidal CdSe/ZnS quantum dots under high pressures, **C. T. Yuan**, Y. C. Lin, Y. N. Chen, Q. L. Chiu, W. C. Chou, D. S. Chuu, W. H. Chang, H. S. Lin, R. C. Ruaan, and C. M. Lin, Nanotechnology 18, 185402 (2007).
5. Fluorescence properties of colloidal CdSe/ZnS quantum dots with various surface modifications, **C. T. Yuan**, W. C. Chou, D. S. Chuu, W. H. Chang, H. S. Lin, and R. C. Ruaan, Journal of Medical and Biological Engineering 26, 131 (2006).
6. Photoluminescence of $ZnSe_xTe_{1-x}$/ZnTe multiple-quantum-well structures grown by molecular-beam epitaxy, Y. T. Shih, Y. L. Tsai, **C. T. Yuan**, C. Y. Chen, C. S. Yang, and W. C. Chou, Journal of Applied Physics 96, 7267 (2004).